# V. Development of Fundamental Technology

## V.1 Core Sampling Technology and Results

(1) Purpose

To understand the in-situ characteristics of the formation containing MH, core samples extracted while maintaining the formation pressure (“pressure cores”) would provide valuable information. Continuous improvement and testing of pressure core sampler (corer) were carried out to recover pressure cores more reliably.

(2) Background

The pressure corer PTCS (Pressure Temperature Core Sampler) was developed in 1995-2000 by JNOC, the predecessor of JOGMEC, and Aumann & Associates (AAI). Tool design has been modified since 2001 (Phase 1 of the project) in order to improve the core recovery rate and workability. By using this coring tool, cores were recovered in the "Tokai-oki to Kumano-nada" exploratory test wells in 2003, and the recovery rate of the pressure cores was 79%, and the pressure retention success rate was 90% of the coring runs [1].
This PTCS was designed on the premise of depressurizing cores on board for observation and analysis purposes. However, since the Pressure Core Analysis and Transfer System (PCATS) was developed by Geotek Ltd., it became possible to observe, analyze and store cores while maintaining pressure. Along with this, Hybrid PCS (Hybrid Pressure Core Sampler) was jointly developed with AAI and the Japan Agency for Marine-Earth Science and Technology (JAMSTEC) as a pressure corer compatible with PCATS.
In July 2012, JOGMEC performed coring using Hybrid PCS and PCATS for the sand-mud alternate layers containing hydrates at the Daini-Atsumi Knoll [2-6]. As a result, the effectiveness of the systems in the characterization of the formation including MH was demonstrated. However, a problem remained regarding the reliability of the pressure holding operation of Hybrid PCS. Therefore, JOGMEC reviewed PTCS, which had already been regarded as an older generation, and decided to make it compatible with PCATS while maintaining the mechanism of the ball valve.
In 2014, PTCSs stored by JOGMEC were transported to AAI, then remodeling work was conducted using some newly created parts compatible with PCATS. This improved tool, HPTC III (High Pressure Temperature Corer III), was tested in a factory, and expected performance was confirmed in a field trial using a land rig in Texas, USA in 2015. Then coring jobs using HPTC III and PCATS were performed in offshore Japan in 2018 during the operation of the supplemental data acquisition campaign, which was conducted after the second offshore production test.

(3) Implementation and results

① Outline and Features of Each Corer

Table 1 compares the specifications of PTCS, Hybrid PCS and HPTC III.

Table 1 Specification of Pressure Corers Used by JOGMEC

| Item | PTCS [1] | Hybrid PCS [2] | HPTC III |
|---|---|---|---|
| Drill pipe OD | 6-5/8” | 5” or 5-1/2” | 6-5/8” |
| Max. pressure of Autoclave | 24 MPa | 35 MPa | 35 MPa |
| Compatibility w/PCATS | No | Yes | Yes |
| Core OD | 66.7 mm | 51 mm | 54 mm |
| Core length | 3 m | 3.5 m | 3.5 m |
| Core bit | 10-5/8" PDC Bit | 10-5/8" PDC Bit | 10-5/8" PDC Bit |

All these corers are rotary coring systems with a wireline-retrievable mechanism. The inner barrel consists of an autoclave to contain the core, and a pressure regulator with accumulated nitrogen gas (Figure 1). When pulling the inner barrel out using a wireline, the autoclave retracts and the ball valve at the bottom of the inner barrel closes. Then the autoclave is pressurized to the set pressure that is ideally above the predicted bottomhole pressure.

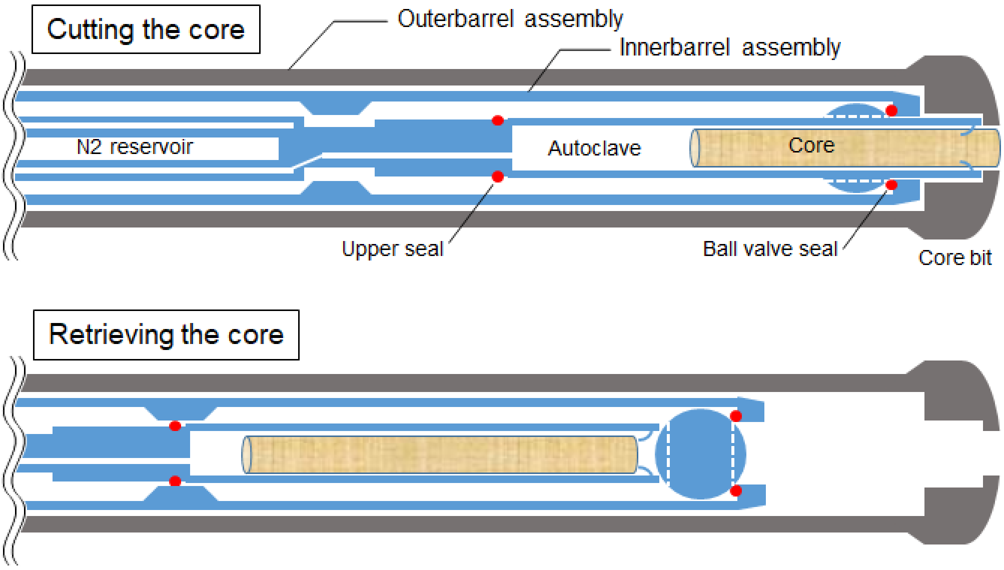


Fig.1 Conceptual diagram showing operation of PTCS and HPTC III

Hybrid PCS was designed for use with general 5 or 5.5 inch drill pipes, considering compatibility with other coring systems used on the drilling vessel Chikyu, such as HPCS (Hydraulic Piston Coring System) and ESCS (Extended Shoe Coring System). Due to this compatibility, the diameter of the inner barrel became smaller than that of PTCS, therefore the design around the ball valve was changed.

On the other hand, the HPTC III is a modified version of PTCS that can be used with PCATS. Therefore, the ball valve design of HPTC III is similar to that of PTCS. In addition, the tool uses the same outer barrel assembly (with the exception of the core bit) and drill pipes. The pressure rating of the autoclave was increased to 5,000 psi and the core diameter was reduced so that the autoclave can fit PCATS.

② Pressure Core Sampling

In July 2012, the year before the first production test, pressure cores were taken from the sand-mud alternate layers containing MH in the Daini Atsumi Knoll area. In the coring well AT1-C, a total of 60m was cored using ESCS and Hybrid PCS. For Hybrid PCS, 18 cores with a total length of 35m were extracted from a 51m section. Among the cores recovered on the ship, eight had over 12MPa, four had over 5.5MPa, and six had less pressure retention [2]. As a result, the core recovery rate was 69%, and the pressure holding success rate over 12 MPa was 44%.

In March-April 2018, coring with HPTC III was performed in Wells AT1-CW1 and AT1-CW2 in the supplemental data acquisition operation of the second production test (Table 2). A total of 49 cores were obtained by drilling a 127.9 m section in two wells, with a total core length of 96.4 m. The pressure of the autoclave at the on-board check was higher than the expected bottomhole pressure (approximately 13 MPa) for 46 cores, and for three cores it was low with pressure between 5-10 MPa. Fig. 2 shows an example of the temperature and pressure history in the autoclave. These data confirmed that all 49 cores were recovered onboard while the hydrate-stable condition was maintained. Summarizing the above, the average core recovery rate was 77%, and the success rate for holding pressure over the bottomhole pressure was 94%.

Table 2 Summary of Results of Pressure Coring in 2018

| | CW-1 | CW-2 |
|---|---|---|
| Date | 2018/4/7 - 4/12 | 2018/3/30 - 4/4 |
| Depth interval (below rotary table) | 1,280.0m-1,330.9m<br>1,339.8m-1,350.9m | 1,286.5m-1,343.7m<br>1,356.6m-1,362.7m |
| Number of cores | 24 (20 + 4) | 25 (23 + 2) |
| Number of successful pressure boost (> bottom hole pressure) | 23 | 23 |
| Total depth interval | 61.9m | 63.3m |
| Total length of cores recovered | 46.1m | 50.3m |

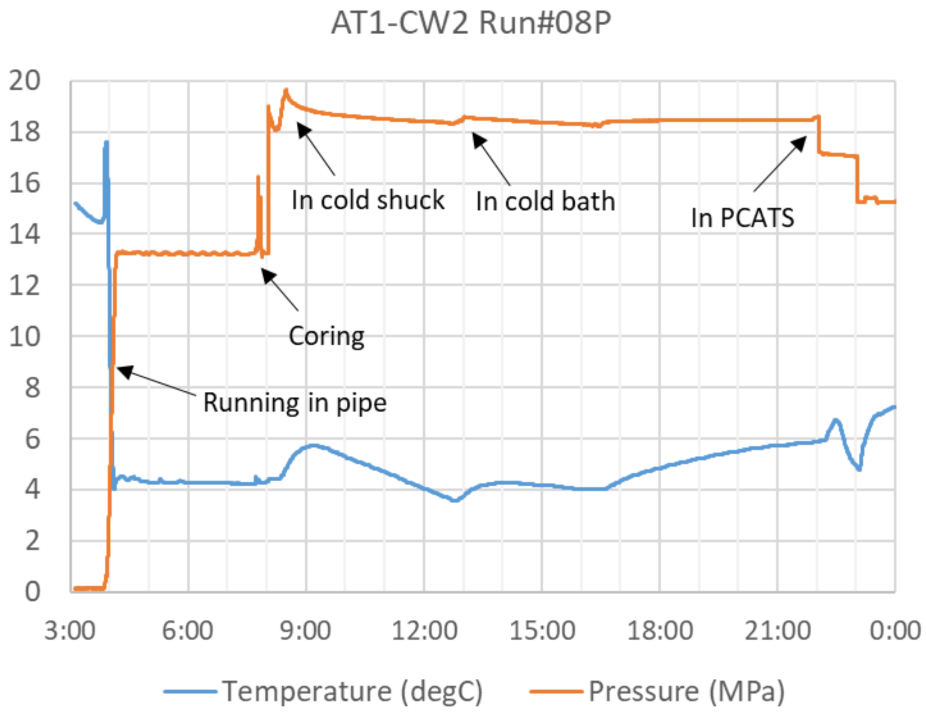


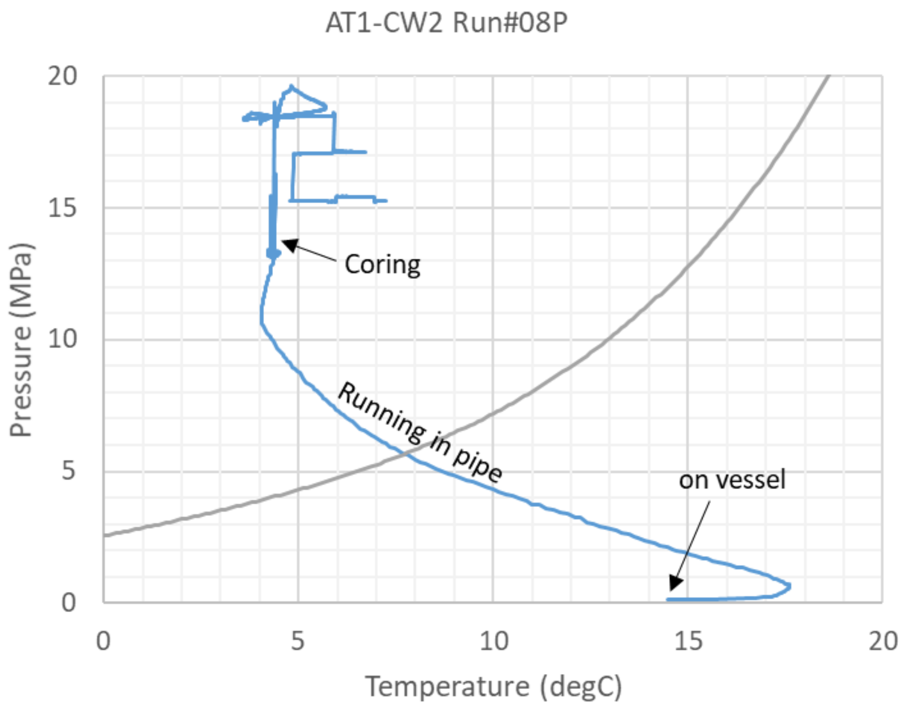


Fig.2 Example of temperature and pressure during coring

(4) Summary and Conclusions

Two different types of pressure corers, Hybrid PCS and HPTC III, were used respectively in the coring campaigns conducted in 2012 and 2018 in combination with PCATS. In both operations, pressure cores were taken, analyzed and preserved on board to characterize the in-situ condition of the formation. HPTC III demonstrated better core recovery rate and successful results in terms of retaining pressure. Although the inner barrel of HPTC III is not interchangeable with that of conventional non-pressure corers, this tool may be the best choice at this time for the coring program where only pressure cores are taken.

References

[1] "Pressure Temperature Core Sampler (PTCS)", Masayuki Kawasaki, Satoru Umezu, Masato Yasuda, Journal of the Japanese Association for Petroleum Technology, 71 (2006), Issue 1, 139-147.

[2] "A new hybrid pressure-coring system for the drilling vessel Chikyu", Y. Kubo, Y. Mizuguchi, F. Inagaki, and K. Yamamoto, Scientific Drilling, Sci. Dril., 17, 37–43, 2014, www.sci-dril.net/17/37/2014/, doi:10.5194/sd-17-37-2014.

[3] "Data report: Hybrid Pressure Coring System tool review and summary of recovery result from gas-hydrate related coring in the Nankai Project", Inada, N. and Yamamoto, K., Marine and Petroleum Geology, 66 (2015) 323-345.

[4] Overview and introduction: Pressure core-sampling and analyses in the 2012–2013 MH21 offshore test of gas production from methane hydrates in the Eastern Nankai Trough, Koji Yamamoto, Marine and Petroleum Geology, 66 (2015), 296-309.

[5] Data report: Hybrid Pressure Coring System tool review and summary of recovery result from gas-hydrate related coring in the Nankai Project, Norihito Inada, Koji Yamamoto, Marine and Petroleum Geology, 66 (2015), 323-345.

[6] Physical properties and sedimentological features of hydrate-bearing samples recovered from the first gas hydrate production test site on Daini-Atsumi Knoll around Eastern Nankai Trough, Kiyofumi Suzuki, Peter Schultheiss, Yoshihiro Nakatsuka, Takuma Ito, Koji Yamamoto, Marine and Petroleum Geology, 66 (2015), 346-357.

## V.2 Pressure Coring and Analysis Technology (Pressure-core Nondestructive Analysis Tools PNATs)

### V.2.1 Introduction

A total analysis system on the methane hydrate sediment cores could be developed to gain an understanding of the geophysical and geo-mechanical properties of methane hydrate reservoirs. Analyses and studies on the pressured cores will be carried at AIST Hokkaido Center in Japan. [1]-[4]

### V.2.2 Pressure-core Nondestructive Analysis Tools (PNATs)

The AIST introduced the Pressure-core Nondestructive Analysis Tools (PNATs), in which the pressure core is handled without depressurizing the pore pressure until core samples are set up in the tools. The PNATs can provide essential reservoir parameters such as permeability, hydrate saturation, X-ray CT image, p-wave response, mechanical properties, and so on, under fully pressurized operation. The following advanced facility and testing tools can be conducted under fully pressurized operation and provide essential reservoir parameters as shown in Table 1 and Fig. 1.

Table 1　Pressure-core Nondestructive Analysis Tools (PNATs) and Analysis Item

| | Under Pressurization | Atmospheric pressure |
|---|---|---|
| Analysis item | Sediment Structure（PNATs-X）<br>Mechanical properties（PNATs-TACTT）<br>Permeability　（PNATs-TACTT）<br>Multiple properties ; P-wave/S-wave/Sh（PNATs-PG/PNATs-AIST IPTC）<br>MH existence（PNATs-PG） | Grain size<br>Particle density<br>Mineral composition<br>Gas volume<br>Hydrate number<br>Hydrate saturation<br>Thermal conductivity |

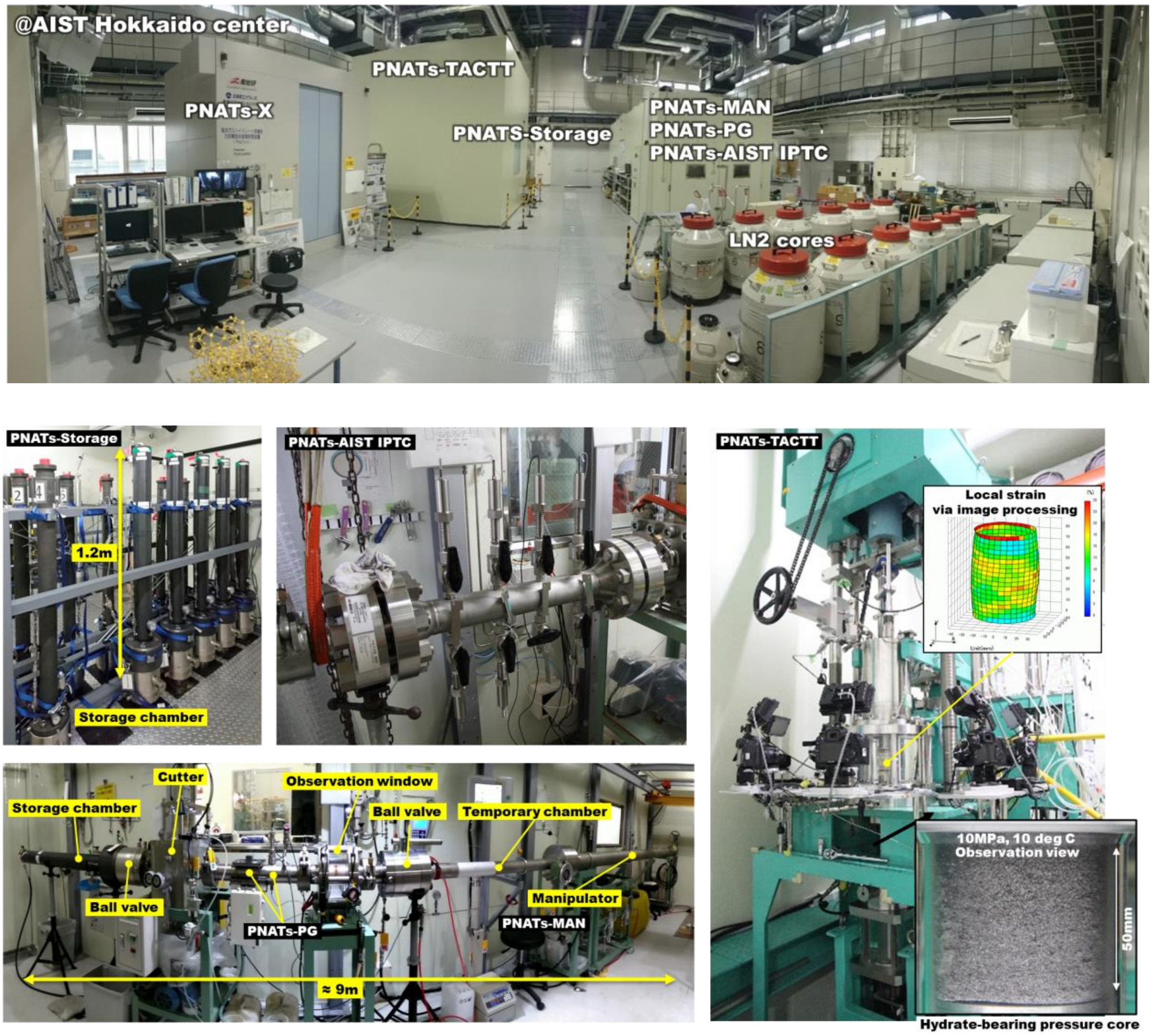


Fig.1 Pressure-core nondestructive analysis tools: PNATs

### V.2.3 Outline of PNAT’s

At first, we measured the sediment structure X-ray CT images of MH cores under pressurized conditions using PNATs-X, and provided P-wave velocity and sediment bulk density by the PNATs-PG. Next, we cut the core including MH, conduct and determine the permeability and geo-mechanical properties using PNATs-TACTT and PNATs-AIST IPTC. After carrying out depressurization, we sample and measure the gas and sand particles, etc. Also, short length cores by LN2 treatment are measured for hydration number, thermal conductivity, etc. We developed the Pressure-Core Nondestructive Analysis Tools (PNATs) to obtain information about many fundamental properties such as permeability, strength, stiffness, compressibility, P and S wave velocities, and thermal conductivity from hydrate-bearing pressure core marine sediments.

References

[1] Yoneda, J., Masui, A., Tenma, N., Nagao, J., 2013. Triaxial testing system for pressure core analysis using image processing technique. Rev. Sci. Instrum. 84, 114503.

[2] Yoneda, J., Masui, A., Konno, Y., Jin, Y., Egawa, K., Kida, M., Ito, T., Nagao, J., Tenma, N., 2015, Mechanical behavior of hydrate-bearing pressure core sediments visualized under tri-axial compression. Marine and Petroleum Geology, 66, 451–459.

[3] Jin, Y., Konno, Y., Yoneda, J., Kida, M., Nagao, J., 2016, In situ methane hydrate morphology investigation: natural gas hydrate-bearing sediment recovered from the Eastern Nankai Trough area. Energy Fuels 30 (7), 5547–5554.

[4] Yoneda, J., Masui, A., Konno, Y., Jin, Y., Kida, M., Katagiri, J., Nagao, J., Tenma, N., 2017, Pressure-core-based reservoir characterization for geomechanics: Insights from gas hydrate drilling during 2012-2013 at the Eastern Nankai Trough, Marine and Petroleum Geology, 86, 1-16.

## V.3 Modeling and Numerical Simulation Technology

### V.3.1 MH21-HYDRES

(1) Introduction

In order to predict the MH dissociation and gas / water production when applying various production methods such as depressurization and heating to MH reservoirs, a numerical simulator that can simulate physical and chemical phenomena specific to MH dissociation / formation behavior is required. However, no commercial simulator capable of simulating gas production from MH reservoirs has existed until now. Hence, the Research Consortium for Methane Hydrate Resources in Japan has been developing Japan's own production simulator (MH21-HYDRES) designed especially for predicting gas production behaviors in MH reservoirs.

(2) Outline of MH21-HYDRES

To produce methane from the MH reservoir, it is necessary to dissociate MH in the sediment by adding external factors from the well and by pumping out the released methane gas from the well. MH21-HYDRES can simulate various phenomena such as dissociation and formation of MH, fluid flow of gas and water, and heat conduction in porous media so that the series of processes from MH dissociation to gas production can be simulated. These phenomena are simulated by numerically solving the governing equations (mass conservation equations of components and energy conservation equation) in which fluid pressure, temperature, and the mass of each component are treated as primary unknowns. At this time, the governing equation is discretized using the finite difference method, and an approximate solution is obtained using the numerical method. The input data required for the simulation are the structure of the reservoir, the reservoir characteristics at the discretization point, the initial condition, well control condition, boundary condition, and so on.

- Reservoir structure: Depth of each layer, grid system, etc.
- Reservoir property: Porosity, absolute permeability, relative permeability, thermal conductivity, etc.
- Initial condition: Formation water and MH saturation, salinity, fluid pressure, temperature, etc.
- Boundary condition: Fluid and thermal flow and non-flow conditions at reservoir model boundaries
- Well control condition: Bottom hole pressure, gas/water production rate, inhibitor injection rate, etc.

(3) Features of MH21-HYDRES

The characteristics of MH21-HYDRES are to be especially designed for use in the development of methane hydrate resources. The main differences from ordinary reservoir simulators designed for the exploitation of conventional oil and gas are as follows (Fig.1):

- Target phases: Gas, water, methane hydrate, and ice
- Target components: Methane, nitrogen, carbon dioxide, water, methanol, and salt
- Able to simulate dissociation / formation of methane hydrate and dissolution / formation of ice based on the equations of kinetics
- Able to simulate the exothermic and endothermic behaviors associated with both dissociation / formation of methane hydrate and dissolution / formation of ice
- Able to shift the three-phase equilibration curve of methane hydrate- methane- water (ice) depending on the concentrations of methanol or salt
- Able to modify the solubility of methane into the water phase by taking into account the salinity concentration
- Possible calculations of the mixed hydrate phases of methane, nitrogen and carbon dioxide as well as methane hydrate
- Introducing the effective permeability and relative permeability as a function of methane hydrate saturation / ice
- Able to handle the analyses of the productivity and the production behavior in various basic production methods and their combinations such as the depressurization, the thermal stimulation, the thermal flooding, the inhibitor injection, the nitrogen injection, etc.

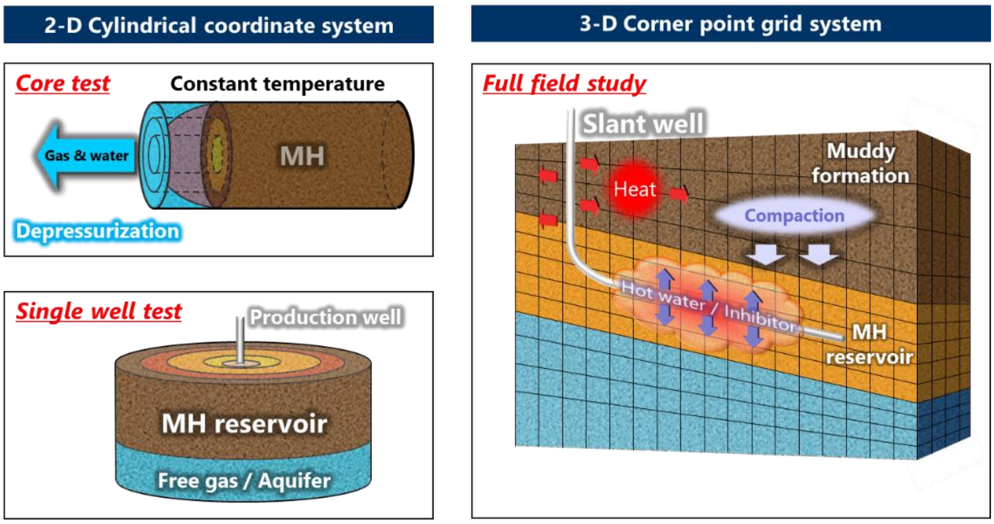


Fig.1 Outline of MH21-HYDRES

(4) Functions of MH21-HYDRES have been improved in Phase 2 and 3

Development of the MH21-HYDRES has progressed to the stage where it can withstand practical use in Phase 1. Development was also continued in Phase 2 and 3 in response to requests for more advanced simulations, such as more detailed test behavior prediction and analysis, and development and evaluation of new production methods. The main functions that were improved in Phase 2 to 3 are as follows:

- Model of carbon dioxide hydrate formation and methane production process with nitrogen / carbon dioxide injection (equilibrium coating model and molecular diffusion model in hydrate)
- Calculation routine for electrical heating method
- Group control function of multiple wells
- Able to handle the optimization method (automatic history matching)
- Development of graphical user interface program for input data creation support
- Result output corresponding to typical oil and gas reservoir viewer format (Fig. 2)

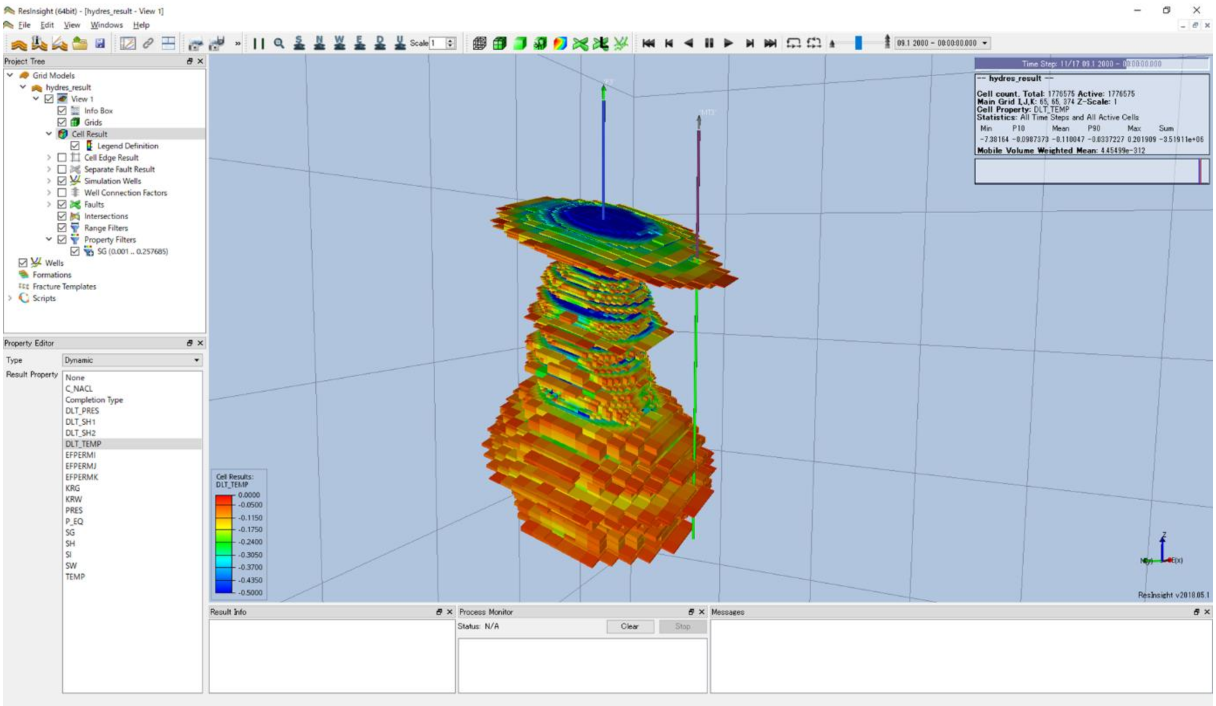

Fig.2 Temperature distribution of 3D model using typical oil and gas reservoir viewer

(5) Achievements of MH21-HYDRES

In the international code comparison project for methane hydrate simulators in Phase 1, MH21-HYDRES has already exhibited superiority in terms of calculation accuracy and calculation stability.

In addition, MH21-HYDRES also has considerable records that have been used in behavioral prediction, and test analysis for various actual fields [1-5]. The amount of gas / water production and the dissociation area of MH predicted by MH-21-HYDRES were extensively utilized for the various objectives before the first and second offshore production tests as follows,

- Selection of production test area
- Selection of the production / observation wells' locations in the test area
- Selection of perforation intervals
- Design of downhole / onboard equipment
- Creation of work guidelines

These simulation results contributed to the success of the first and second offshore production tests in Japan.

Furthermore, MH21-HYDRES has been used in a wide range of applications such as production behavior prediction for economic estimation, and examination of new production methods [6-7].

(6) Investigation of the first and second offshore production tests by MH21-HYDRES

In order to investigate the cause of the discrepancy between the prediction results and the actual production behaviors in the second offshore production test, a quick simulation analysis was conducted assuming various phenomena by immediately taking the test data during the test (Fig. 3). In addition, MH-HYDRES was also used for post-analysis of the production test such as "history matching" in which reservoir parameters are modified to reproduce gas/water production and thermal observation data. The results of the post-analyses were extensively utilized in various situations such as the elucidation of MH dissociation behavior and other phenomena in the reservoir when applying the depressurization method on a field scale, and in a review of the reservoir model (Fig. 4). In addition, throughout the post-analysis of the production test, it is suggested that the salinity of the formation water depends on formation depth. In order to take into account the relationship between salinity and depth, a new function for defining tables (depth vs. salinity) was added to MH21-HYDRES, which contributed to the improvement of the simulator (Fig. 5).

Various factors were understood through the post-analysis. Among those new findings, the following three items in particular should be considered in detail in the future.

1. It is difficult to reproduce the high gas production rate at a low degree of depressurization observed in the P2-Well only by considering the effect of the salinity concentration and the influence of the chemical agent injected into the P2-Well before the production test. (We need to introduce other assumptions to reproduce the production behavior in the P2-Well.)
2. There is a high possibility that the tendency of absolute permeability and initial effective permeability in terms of water changes in between P2-Well and P3-Well, which are only about 60 m apart.
3. There is a possibility that the gas and water production behavior of P3-Well and the temperature and pressure behavior of the monitoring well could be reproduced by assuming the skin formation in the vicinity of the production well.

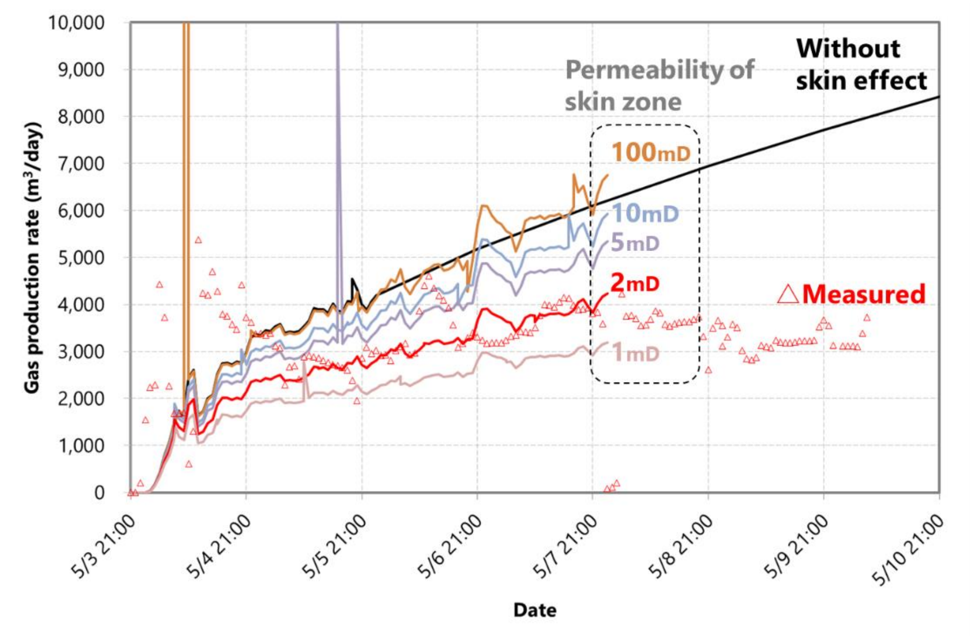


Fig. 3 Immediate analysis of second off-shore production test (sensitivity analysis for skin influence in vicinity of well)

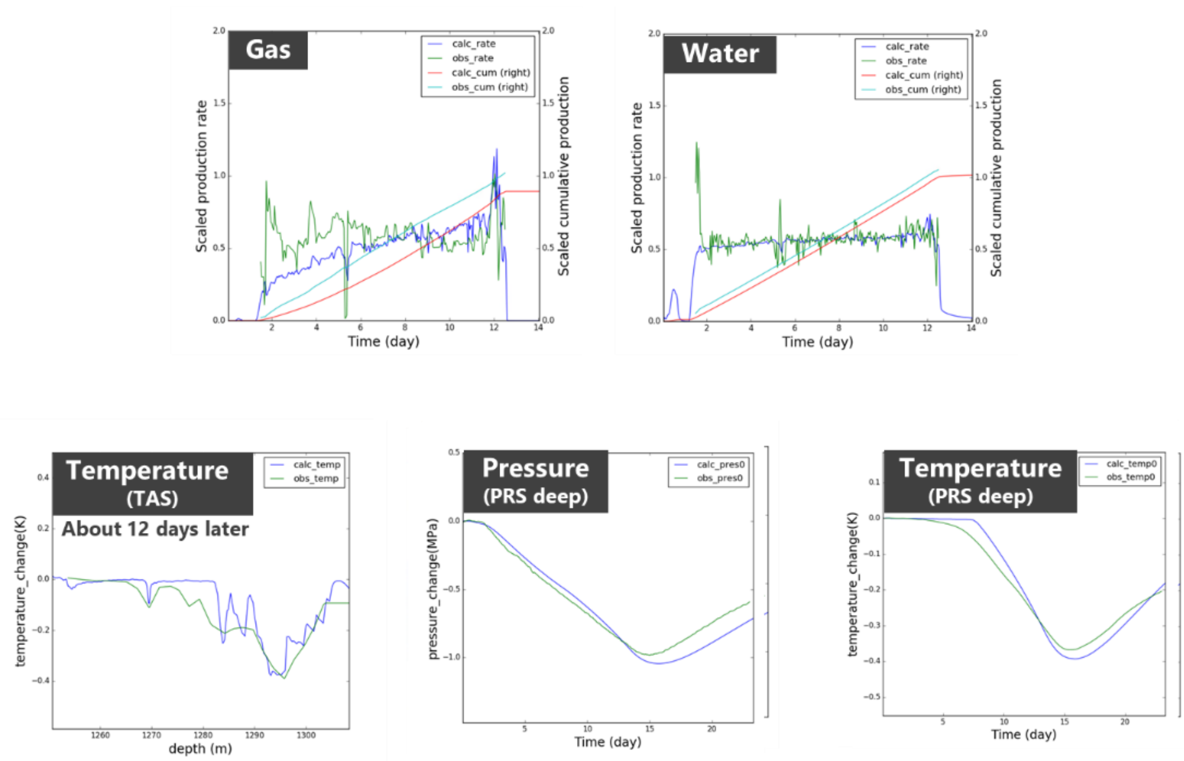


Fig. 4 Results of P3-Well in second off-shore production test (calculation example)

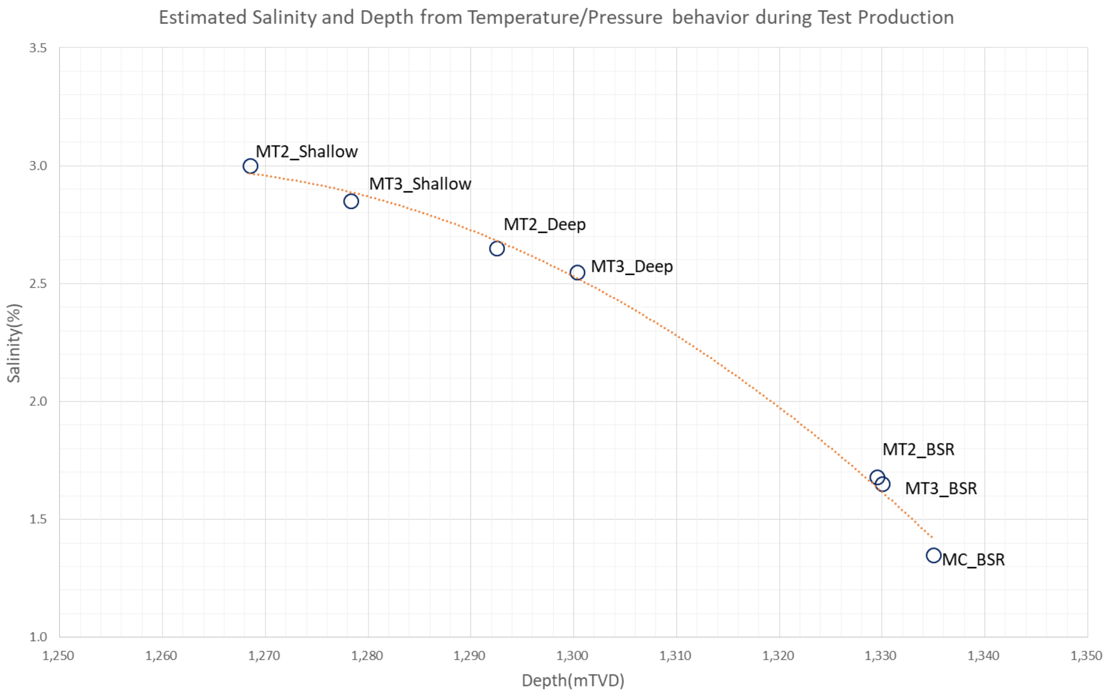


Fig. 5 Relationship with salinity concentration and depth

(7) Summary and future issues in this section (V.3.1: MH21-HYDRES), the overview of the functions of MH21-HYDRES, the improvement / enhancement of the functions of the simulator in Phase 2 and Phase 3, and the application of the simulator to various problems were introduced. In order to deal with complicated analyses such as those mentioned in (6), further development of the simulator including speeding up of the calculation and enhancement of the pre-existing functions, is necessary. For example, there is not enough information to explain the reason why in the current post-analysis of the production test in the P2-Well, gas production over 10,000 $m^3$/D was observed. (It seems that the three-phase equilibrium curve of MH-methane-water drastically shifted to the high-pressure region during the P2 production test for some reason. However, the reason for the shift has not yet been fully clarified.) To explain the cause of the high gas production rate in the P2 production test, we need to introduce a new reservoir model based on the new assumption such that an area with extraordinarily high salinity exists adjacent to the P2-Well. However, this kind of 3D reservoir simulation still requires several days for a single run. We need to keep improving the calculation speed of MH21-HYDRES to address the complicated problems in the actual field.

In addition, several data obtained in the production tests suggests that the current model constitutive equation regarding permeability change during MH dissociation may not represent the actual permeability change in the actual field. It is also necessary to improve these kinds of constitutive equations in MH21-HYDRES in order to further improve prediction accuracy.

References

[1] M. Kurihara, A. Sato, H. Ouchi, Y. Ohbuchi, Y. Masuda, H. Narita, T. Ebinuma, and T. Fujii, 2009: “Examination on gas producibility from Eastern Nankai Trough methane hydrate resources”, 石油技術協会誌, Vol. 74, No. 4, pp. 311-324

[2] H. Ouchi, M. Kurihara, A. Sato, Y. Masuda, H. Narita, T. Ebinuma, T. Saeki, T. Fujii, T. Kobayashi, and N. Shimoda, 2010: “Construction of 3 dimensional methane hydrate reservoir model in Eastern Nankai Trough and prediction of production test performance”, 石油技術協会誌, Vol. 75, No.1, pp. 72-83

[3] M. Kurihara, A. Sato, K. Funatsu, H. Ouchi, Y. Masuda, H. Narita, and T. Collett, 2011: “Analysis of formation pressure test results in the Mount Elbert methane hydrate reservoir through numerical simulation”, Marine and Petroleum Geology, Vol 28, Issue 2, Feb 2011, pp. 502-516

[4] M. Kurihara, A. Sato, K. Funatsu, H. Ouchi, K. Yamamoto, M. Numasawa, T. Ebinuma, H. Narita, Y. Masuda, S. Dallimore, F. Wright, and D. Ashford, 2010: “Analysis of Production Data for 2007/2008 Mallik Gas Hydrate Production Tests in Canada”, SPE International Oil and Gas Conference and Exhibition in China, 8-10 June, Beijing, China, SPE 132155

[5] Y. Konno, T. Fujii, A. Sato, K. Akamine, M. Naiki, Y. Masuda, K. Yamamoto, and J. Nagao, 2017: “Key Findings of the World's First Offshore Methane Hydrate Production Test off the Coast of Japan: Toward Future Commercial Production”, Energy & Fuels, Vol. 31, No.3, pp. 2607-2616

[6] Y. Konno, Y. Masuda, Y. Hariguchi, M. Kurihara, and H. Ouchi, 2010: “Key Factors for Depressurization-Induced Gas Production from Oceanic Methane Hydrates”, Energy Fuels 24, pp. 1736-1744

[7] Y. Konno, Y. Masuda, K. Akamine, M. Naiki, and J. Nagao, 2016: “Sustainable gas production from methane hydrate reservoirs by the cyclic depressurization method”, Energy Conversion and Management, Vol. 108, pp. 439-445

### V.3.2 COTHMA

(1) Summary

Depressurization is considered an effective method for producing methane gas from a methane hydrate layer. Because of large pressure drops produced by depressurization in the earth’s sediment, depressurization is estimated to have various effects including a change in consolidation of a well’s vicinity when producing methane hydrate. In addition, the process of producing gas from methane hydrate layers involves dissociating the solid methane hydrate in the sediment and transforming its state into water and methane gas. This causes the strength of the layers to degrade, which in turn produces deformations in the sediment. Therefore, we predict the deformations and stress states of the sediment during methane hydrate production and developed a **co**upled **t**hermo-**h**ydro-**m**echanical **a**nalysis (COTHMA) sediment deformation simulator that simulates dissociation and formation of methane hydrate in the deformation of multiphase porous media [1]. COTHMA uses a finite element method complete with thermal conduction based on changes in temperature derived from the dissociation and formation of methane hydrate (in addition to its stress/deformation) and osmotic flow derived from the change in water pressure. The purpose is to evaluate the impact on the soundness of a well.

The simulator allows one- to three-dimensional (3D) analysis including two-dimensional (2D) plane strains, 2D cylindrical coordinate systems, and 3D Cartesian coordinate systems. We also achieve high precision by successively adding constitutive equations of a stress-strain relationship based on recent findings and repeated tests through functional enhancements and results of in-house experiments.

(2) Functions and Features of Sediment Deformation Simulator

With COTHMA, we were able to handle methods of gas production using the methods of depressurization, well-heating, and hot-water circulation, as well as heterogeneous gas injection methods. In addition, through analysis, we could consider changes in the phase states and physical properties listed as follows.

- Change of phase states through dissociation/regeneration of methane hydrate and generation/melting of ice
- Deformation in the sediment layer and change in strength characteristics due to phase changes
- Change in the permeability of sediment layer due to phase changes and consolidation.

In addition, we could fix the displacement, pressure, and temperature or change it with time based on the boundary value problem. We could assign the load, flow rates (of gas and liquid phases), and rate of heat flow for the nodes and elements. The predicted deformation in the sediment was proposed in relation to COTHMA's simulator, which is necessary for evaluating the well's soundness. Because the stress-strain relationship of the methane hydrate layer and the well's materials dominate the results of the evaluation, we introduced various constitutive equations that reflect the mechanical test results in order to achieve a high level of precision with the simulator. All constitutive equations of a methane hydrate layer allow effects to be considered due to methane hydrate's saturation factor, and they are compatible with the following models: a linear model that considers the confining pressure dependence, a model that considers post-breakage non-linear characteristics, a time-dependent non-linear model, and an elastoplastic model that considers plastic deformation. In addition, we introduce an elastoplastic model that can predict the necessary plastic strain after the soundness of the well's metal and cement materials is evaluated. Table 1 shows the constitutive equations introduced in the simulator.

Table 1 Constitutive Equations Introduced in the simulator

| Constitutive Equations | Soil Material[1)] | Cement | Metal |
|---|---|---|---|
| Elastic Model | Linear Model<br>Confining Pressure-Dependent Linear Model | Linear Model | Linear Model |
| Elastoplastic Model | Modified Sekiguchi-Ota Model<br>Son-Matsuoka Model<br>Mohr-Coulomb Model<br>Drucker-Prager Model | Mohr-Coulomb Model<br>Drucker-Prager Model | Tresca Model<br>von Mises Model |
| Non-Linear Model | Duncan-Chang Model<br>Modified Duncan-Chang Model<br>Composite Geomaterial Model<br>Viscoelasticity Variable-Compliance Model | | |
| Non-Linear Model[2)] | Bilinear Contact Surface Model<br>Variable-Compliance Contact Surface Model | | |

1) We consider the dependency for the constitutive equations and methane hydrate's saturation factor for soil material
2) Constitutive equation for the joint element

### (3) Verification and Results of Simulator

Due to the development of a component in COTHMA used to verify the mechanical test results of core specimens that include methane gas, the simulator could accurately represent the behaviors of methane hydrate-inclusive sediment deformation (Fig. 1). In addition, we improved the simulator's accuracy by installing mechanical testing equipment capable of testing in a high-pressure-maintained state and that achieved greater mechanical parameter precision and optimized constitutive equations based on the test results.

Furthermore, to achieve a higher level of accuracy of the well's model when evaluating its soundness, we performed detailed modeling based on the on-site well as well as indoor model testing to obtain the strength of the contact surface between the sediment (sand or mud layer) and casing or cement. For example, regarding the strength of the contact surface between the casing and cement, we derived an empirical formula that uses the effective confining pressure as a parameter [2].

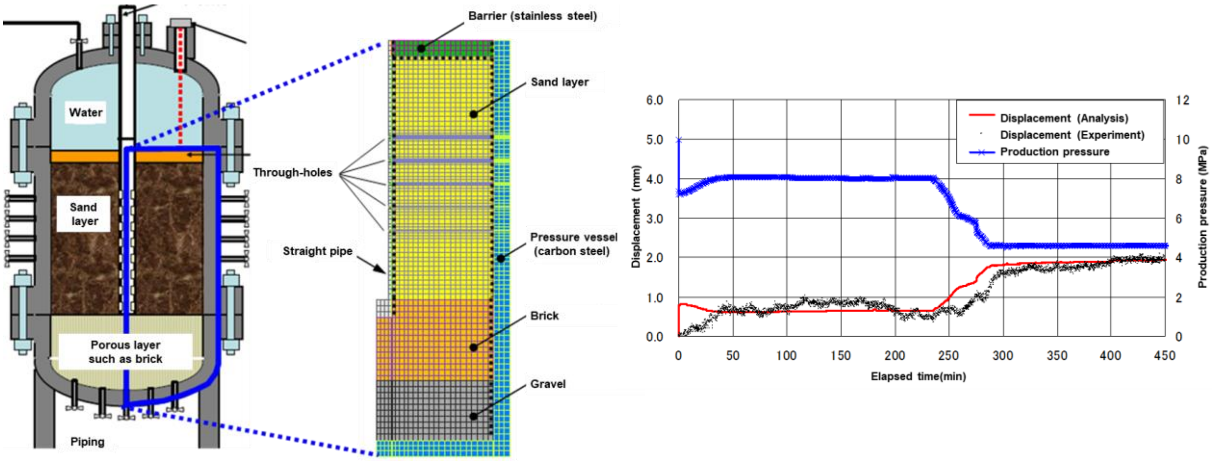


Fig.1 Reproduction analysis of depressurized gas production tests using large indoor testing equipment.

These results were assessed through an analysis that uses a numerical ground model formulated based on the ground information of offshore production testing sites. For example, Fig. 2 shows a sample analysis of sediment deformation and the stress states of the well's surroundings during the first offshore production test. According to analytical results, sediment deformation, which is primarily caused by the consolidation deformation in conjunction with methane hydrate dissociation and increased effective stress, occurs mainly in the depressurized section.

(4) Simulator Acceleration

The simulator operates with Windows and Linux operating systems, where the Linux version features a PETSc solver with parallel computing capabilities. When compared to the direct method and calculation speed with a model of 20,000 nodes, the simulator achieves an acceleration of two times, and more than 100 times for 2D and 3D analyses, respectively.

(5) User Interface Development

We attempted to optimize the analysis processes by developing a postprocessor that postprocesses the results of the analysis as well as a preprocessor that supports the creation of COTHMA's input data. In addition, we created a graphical user interface screen for these preprocessors, which makes the simulator more user-friendly.

(6) Conclusion

We described the essential features and functions of the COTHMA sediment deformation simulator. In addition, we produced enhancements such as a user interface, and we improved various functions while attempting to achieve increased simulator reliability based on the results of on-site testing. Long-term wide-area verification through an actual implementation as well as improved precision to the sediment deformation simulator are needed.

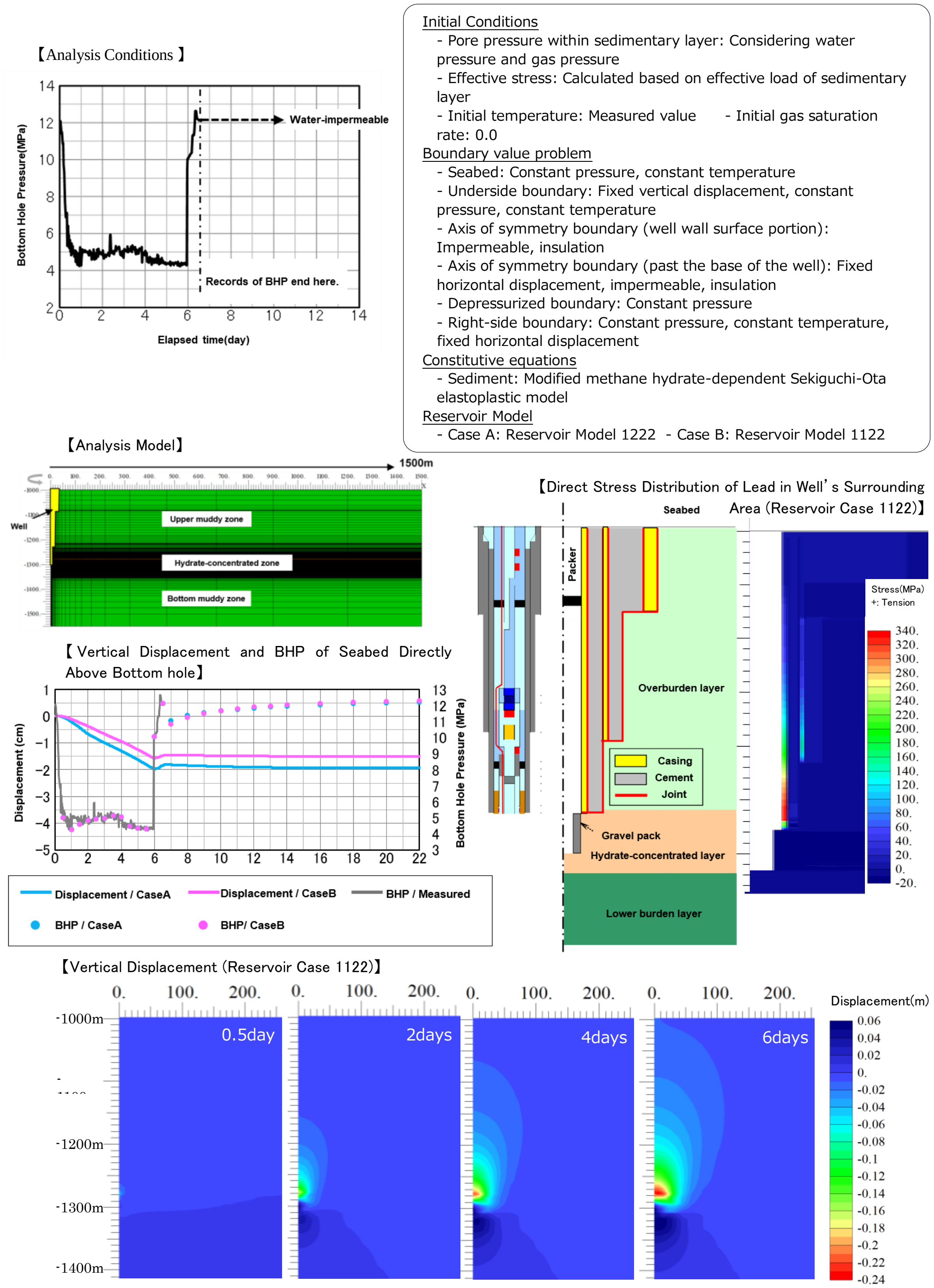


Fig. 2 Analytical conditions and results (displacement, stress distribution) of first offshore production test

References

[1] J. Yoneda, A. Takiguchi, T. Ishibashi, A. Yasui, J. Mori, M. Kakumoto, K. Aoki, and N. Tenma、 2018 (accepted): "Mechanical Reaction of Reservoir and Well Completion of the First Offshore Methane Hydrate Production Test at the Eastern Nankai Trough: A Coupled Thermo-Hydro-Mechanical Analysis," SPE J.

[2] M. Kakumoto, J. Yoneda, K. Miyazaki, N. Tenma, K. Aoki, and R. Itoi 2013: “Basic Study on the Frictional Strength between the Casing and Cement in a Methane Hydrate Production Well,” Journal of MMIJ, Vol. 129, No. 4, 116–123

### V.3.3 Geomechanics-related Studies

The in-situ MH dissociation that takes place through depressurization is an event involving large degrees of pressure and effective stress, and may cause several types of mechanical phenomenon. **Fig. 1** depicts examples of drilling, gas production, and safety issues. To predict the phenomenon and reduce any kinds of risks, gathering and analyses of data related to the mechanical conditions in formations should be combined with modeling techniques.

In the case of an MH study, a specific point is that the formation is basically unconsolidated, and that mechanical parameters depend on the state of MH in formation pores, and consequently, data acquisition and modeling techniques should take these facts into account. In the MH21 consortium study, various geomechanics-related studies have been conducted from many different viewpoints. In this section, a number of examples are described.

(1) Information About Geomechanical Conditions and Their modeling

① Stress Evaluation

To determine six components of the stress tensor, it is necessary to combine several techniques, however, the applicability of some technologies has not been proven in MH-bearing unconsolidated sediment.

During the first offshore production test, ASR (Anelastic Strain Recovery) method was applied with Diametrical Core. Deformation Analysis (DCDA) to the extracted core samples (Nagano et al., 2015), along with the image log-based borehole breakout method. The result revealed that the maximum horizontal stress direction in the Daini Atsumi area varied among boreholes, however, the difference between maximum and minimum horizontal stresses was small, and the stress regime was the normal fault type. The obtained result matches the analysis result of log-derived analysis gathered during Phase 1 (Yamamoto et al., 2006) (**Fig. 2**).

② One Dimensional Mechanical Earth Model (1D MEM)

Log-core correlation-based 1D MEM modeling was performed based on the data of each drilled borehole. In the studies conducted during phase 2 and 3, the procedure to determine the parameters for Modified Cam-Clay (MCC) model (the pre-consolidation pressure, $P_{c0}$; the hardening parameter, $\chi$; the slope of the swelling line, $\kappa$; the slope of the critical state line, $M$) was developed in order to create an appropriate model for unconsolidated sediments. To determine six components of the stress tensor, it is necessary to combine several techniques, however, the applicability of some technologies have not been proven in MH-bearing unconsolidated sediment.

**Fig. 3** indicates the developed 1D MEM for AT1-P2 and P3 with results of break-out analysis using the 1D MEM in comparison with actual measurements of hole diameter. The analysis results have a reasonable match with the real hole-enlargement situation in which a large degree of the enlargement was measured in AT1-P2.

③ Three Dimensional Mechanical Earth Model (3D MEM)

Regarding information to evaluate the heterogeneity of physical parameters in three-dimensional spaces, only seismic data is available and the resolution is 25 m. To create a numerical grid for the geomechanical simulation that requires a few centimeters to meters of resolution from low resolution seismic data, a downscaling technique is necessary. In this study, an application of Bayesian optimization was attempted using the following steps.

The relationship between the mechanical properties and measurable logging parameters such as MH/gas saturation, overburden stress, porosity, clay contents, etc. are determined by the equations in the previous part.

A linear relationship between the seismic velocity ($V_p$) and log-derived parameters (values to be calculated, such as hydrate fraction, $s^{tot}_{\mathrm{hyd}}$; gas fraction, $s^{\mathrm{tot}}_{\mathrm{gas}}$; porosity φ; effective stress, $p_e$; clay content $v_{\mathrm{cl}}$) is assumed with weights on each parameters $c_n$., as follows:

$$V_p=c_o+c_1s^{tot}_{\mathrm{hyd}}+c_2\varphi+c_3p_e+c_4v_{\mathrm{cl}}+c_5s^{\mathrm{tot}}_{\mathrm{gas}}$$

A relationship between the seismic velocity vector ($\boldsymbol{a}_0$, known value) on the seismic grid (resolution is 25m) and log-derived physical parameter vector on the numerical analysis grid (resolution of a few meters) is written as an observation equation: $Am+e=a_0$

where $e$ is an error vector to be minimized (**Fig. 4**).

In the model, the physical and seismic properties on the trajectory of the boreholes are also applied to the known and unknown vectors. The Bayesian optimization procedure is used to minimize the error vector $\boldsymbol{e}$ under the restriction of some prior information (Tarantola, 1987).

Some three-dimensional mechanical simulations have been conducted to analyze the possible operational and environmental risks of the planned offshore production test. **Figs. 5 and 6** show analysis results of the MH dissociation effect on the fault activation at a test candidate site (not Daini Atsumi) (Qiu et al., 2012) and estimated stress conditions in the vicinity of the wellbore in the Daini Atsumi Knoll.

This work has been conducted in collaboration with Schlumberger.

(2) Constitutive Modeling of MH-bearing Soil and its Upscaling Procedure

A critical state soil mechanics model based on the modified Cam-Clay model was developed (Uchida et al., 2012) with a team from the University of Cambridge to include the effects of MH in pore spaces on mechanical behaviors.

To model the finely laminated turbidite sediments with large grid size, an upscaling procedure incorporating a homogenization technique is applied using transverse isotropy of MCC (Wheeler, 2003; Wongsaroj, 2006) and applied to the constitutive model. Furthermore, a homogenization procedure of hydraulic and thermal properties were developed (Zhou et al., 2018a). During the homogenization procedure, 10 parameters in the model are gradually optimized through the comparison of large grid mode with fine grid models with different conditions (homogeneous/heterogeneous host material and homogeneous/heterogeneous MH distribution, and different stress states, **Fig. 7**).

**Fig. 8** shows how the stress passes in the formation during the depressurization and MH dissociation processes around a borehole, and the horizontal contraction of the sediment and large shear strain in the early stage, isotropic compression during the dissociation stage, and compaction of the reservoir in the post dissociation stage were calculated (Zhou et al., 2018b).

(3) Effects of Drilling Operation

In many borehole stability studies, the stress condition changes that occur during drilling operations have been ignored. However, the effects cannot be ignored in the case of MH in weak sediments. In particular, the effects of cementing operations including water absorption/hydration processes and contraction of cement as well as hydration heat effect should not be considered negligible. Such effects have been studied using actual data of cement used for the offshore production tests (Sasaki, et al., 2018a). The detailed drilling process was also modeled (Sasaki, et al., 2018b) and the occurrence of the plastic strain during the drilling operation and significant stress alternation during the cement hydration process were calculated (**Fig. 9**). This work was also carried out with collaboration from The University of Cambridge and the University of California, Berkeley.

(4) Sand Production Modeling

Sand production is a relatively common obstacle involved in gas production from MH in unconsolidated formations. The basic idea of sand production in the oil industry is based on the brittle failure of the rock around borehole and perforation tunnels based on the theory of elasticity. However, sand production in the

MH reservoir must have a different mechanism due to the soft and weak nature of the host sediments.
Based on the developed MCC model, the occurrence of movable solids (detachment) and transport of solids with fluid are modeled with Technion and the Rensselaer Polytechnic Institute (Uchida et al., 2016a). The model assumes that the sand detachment can happen when hydraulic gradient exceed a defined critical value ($i^{crt}$) and the volume of the sand is related to the shear strain ($\varepsilon_d$).
History matching was carried out as part of the sand production event of the first production test (Uchida et al., 2016b) and the produced volume and occurring intervals closely matched the observation (**Fig. 10**).

(5) MICP (microbiologically induced calcite precipitation) Application For Sand Control
One possible method of mitigating the risk of sand production is soil solidification. However, industrially available technologies have been developed for deep and high temperature conditions and are not applicable to cold (< 15 deg C) shallow water sediments. If the biological techniques, MICP-using indigenous species, is applicable, relatively cheap application may be possible. Another advantage is that the extent of the solidified zone can be large due to relatively slow reaction time, and permeability can be controllable. This is an important feature because the permeability of the production zone should be kept high in the production zone, but it should be reduced to seal the water producing interval.
With the collaboration of the University of Cambridge and Toyama Prefectural University, a number of studies including about the effectiveness of current technologies using aerobic species in anaerobic conditions below deepwater (Jiang et al.,2016), evaluation of sand control effects using techniques based on laboratory studies (Jiang et al., 2018) (**Fig. 11**) were carried out. Evaluation of the indigenous species using core samples taken in the offshore production test site have been conducted using 2012 and 2018 pressure cores. Test results have shown positive results and some useful species have been discovered in the taken samples **(Fig. 12)**.

(6) Observation of Sand Production Processes by X-ray CT
How to visualize sand production behind the wellbore surface is an important research subject that will support understanding of the mechanism of the phenomena. JOGMEC and Tohoku University have jointly attempted real-time observation of the sand production process using an X-ray CT device and a carbon fiber-reinforced pressure vessel (Ito, 2016).
The following studies have been carried out:

1) Establishment of the study procedure and devices
2) Observation of the formation structure change due to sand production
3) Analysis on the relationship between the screen opening and sand production
4) Evaluation of the shape memory polymer (GeoFORM™) for Nankai Sand
5) Evaluation of the effect of gas in fluid on the sand production

The test device used is shown in **Fig. 13,** and an example of a typical sand production process and sample observed by X-ray CT are shown in **Fig. 14**. An important discovery was that a sand structure with high permeability streaks (an onion-like structure) can be created around the perforation and stabilize the sanding, perhaps due to the reduction of pressure gradient there. (**Fig. 15**)

(7) Risk Analysis of Seafloor Instability

Dissociation of MH in the subsea sediment leads to the reduction of formation strength. Pressure and buoyancy generated by the generated gas may lead to effective stress reduction. Combining these effects may increase the risk of seafloor instability and subsequent landslides.

The test site of the first and second offshore production tests in the Daini Atsumi Knoll located under the mass transport materials. Relatively large landslide scars are observed in the west of the test site (**Fig. 16**). In addition, the site is close to the epicenter of the anticipated Tonankai Earthquake (Mw > 8). Even though the landslide is not an artificial cause, it may damage subsea devices and test platforms, thus a risk analysis of both artificial and natural reasons was conducted with collaboration from Norwegian Geotechnics Institute (NGI), an organization that participated in the risk analysis of the Storegga slide and Ormen Lange gas field.

The study was carried out in three steps (Kvalstad, 2010):

1) Risk by natural causes by subsea topography and earthquakes (**Fig. 17**)
2) Effects of the MH dissociation (**Fig. 18**)
3) Tsunami analysis caused by the worst case scenario

The result suggested that the factor of safety (FoS) in some steep locations at the headwall of the slide scars is less than 1, and the assumed combination of the Tokai, Tonankai, and Nankai earthquakes may have caused large plastic strains to occur at shallow depths below the seafloor, however, the effects of MH dissociation in the offshore production test scale is minor because the MH reservoir exists around 300 m below the seafloor, which is far deeper than possible slide planes.

(8) Conclusions and Way Forward

During Phase 2 and 3 studies, data acquisition and analyses, and development of the 1/3D mechanical earth model, and numerical simulation studies were carried out mainly for the offshore test site. Currently, few real mechanical response data are available, and it is difficult to verify the results of modeling studies.

In the next stage, it will be necessary to combine the study with mechanical testing of core samples, and data acquisition in the reservoir using strain measurement, etc. for more integrated studies to evaluate the mechanical effects on gas production and safety.

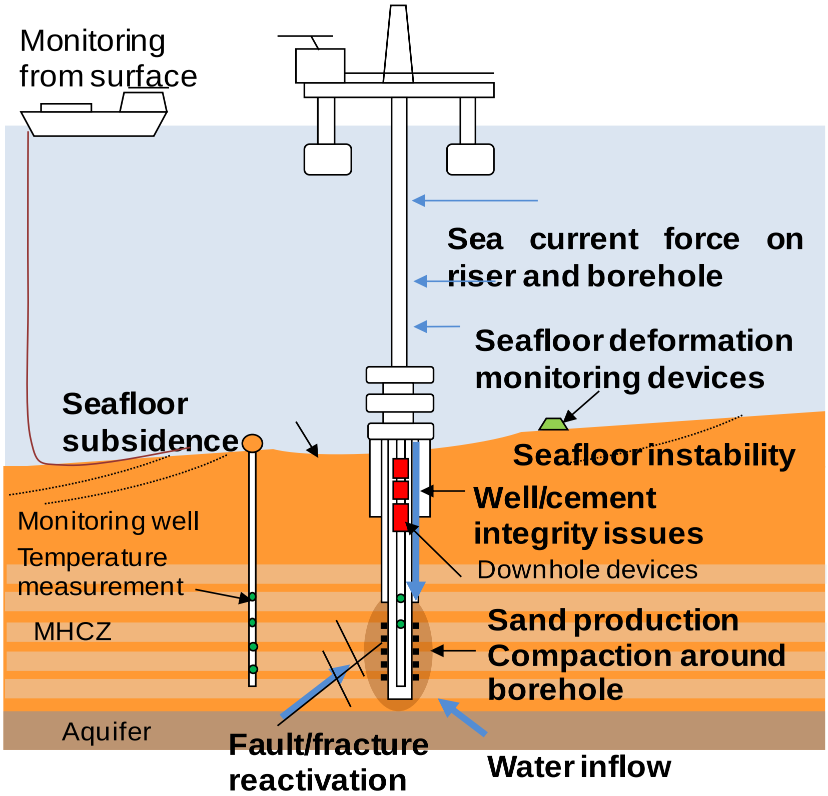


Fig. 1 Possible Geomechanics-related issues under MH dissociation conditions.
(MHCZ: methane hydrate concentrated-zone)

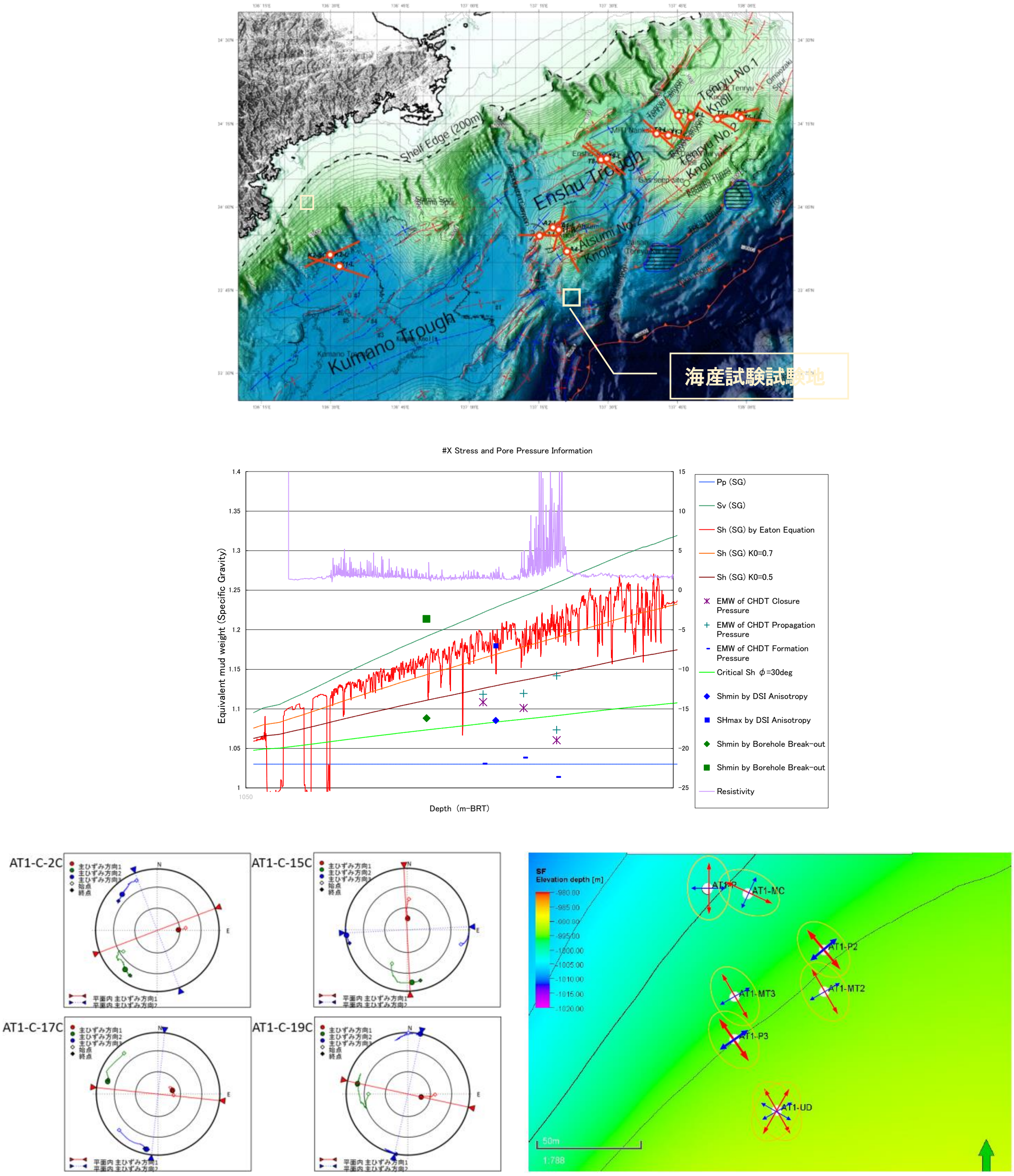


Fig. 2 Log (breakout direction) -derived maximum stress orientation (Top, Yamamoto et al., 2006) and stress gradient data in the Daini Atsumi borehole (middle) and ASR derived stress direction and anisotropy by ASR from pressure core samples (bottom, Nagano et al., 2015)

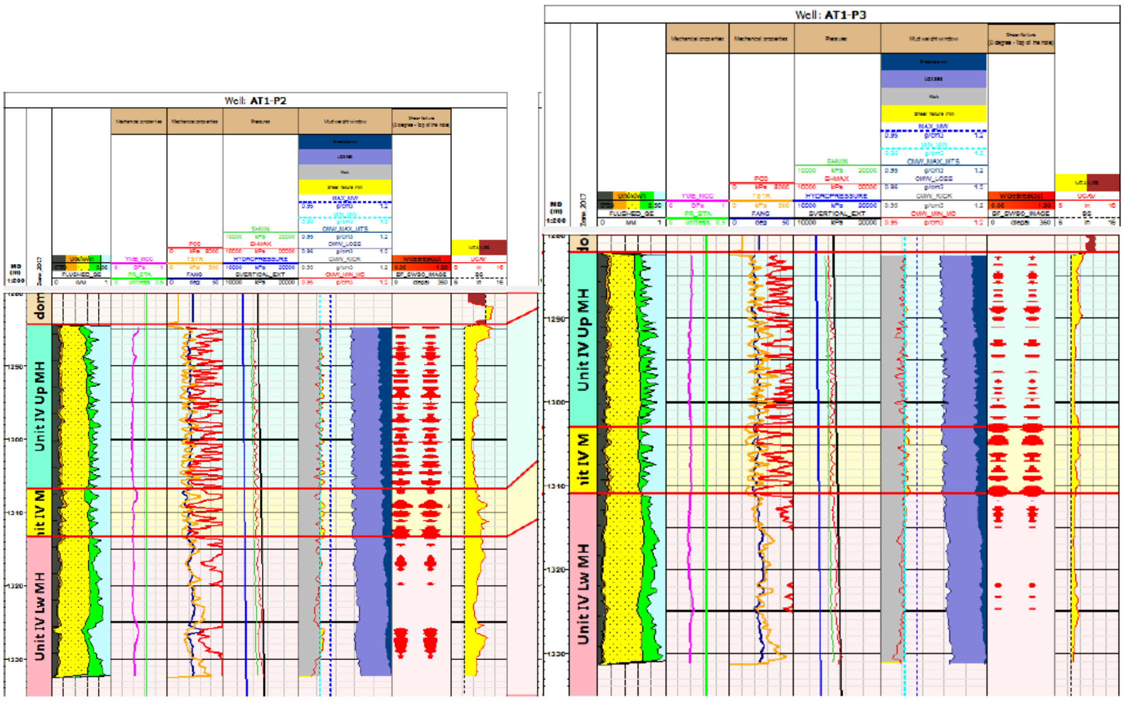


Fig. 3 1D MEM of AT1-P2/P3 wells and breakout results with actual hole enlargement data.

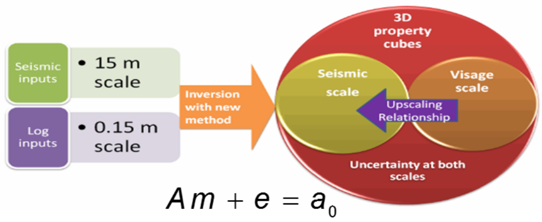


$$Am + e = a_0$$

*m* : Unknown vector; Seismic velocity and mechanical properties on FEM nodes

$a_0$ : Know data vector, Seismic velocity on seismic grid and log data points on well

*e* : Error vector with Gaussian distribution

Posterior probability（probability of $a_0$ when *m* is given)

$$P(\mathbf{a0}\,|\,\mathbf{m}) = ((2\pi)^n |\mathbf{C_D}|^{-\frac{1}{2}} Exp\left[-\frac{1}{2}(\mathbf{a0}-\mathbf{Am})^T \mathbf{C_D^{-1}}(\mathbf{a0}-\mathbf{Am})\right]$$

Prior probability of m: considering physical limitation and expected mean value ($m_0$)

$$P(\mathbf{m}) = ((2\pi)^{nm} |\mathbf{C_M}|^{-\frac{1}{2}} Exp\left[-\frac{1}{2}(\mathbf{m}-\mathbf{m_0})^T \mathbf{C_M^{-1}}(\mathbf{m}-\mathbf{m_0})\right] \quad 15$$

Fig. 4 The process of Bayesian optimization-based downscaling. ***m*** is a vector of unknown values (petro-physical parameters) and $\mathbf{a}_0$ is the seismic velocity vector. Covariant matrix $C_D$ is defined using distribution of seismic velocity. Some prior knowledge and physical limitations of the petro-physical parameters are considered in the prior probability of ***m***.

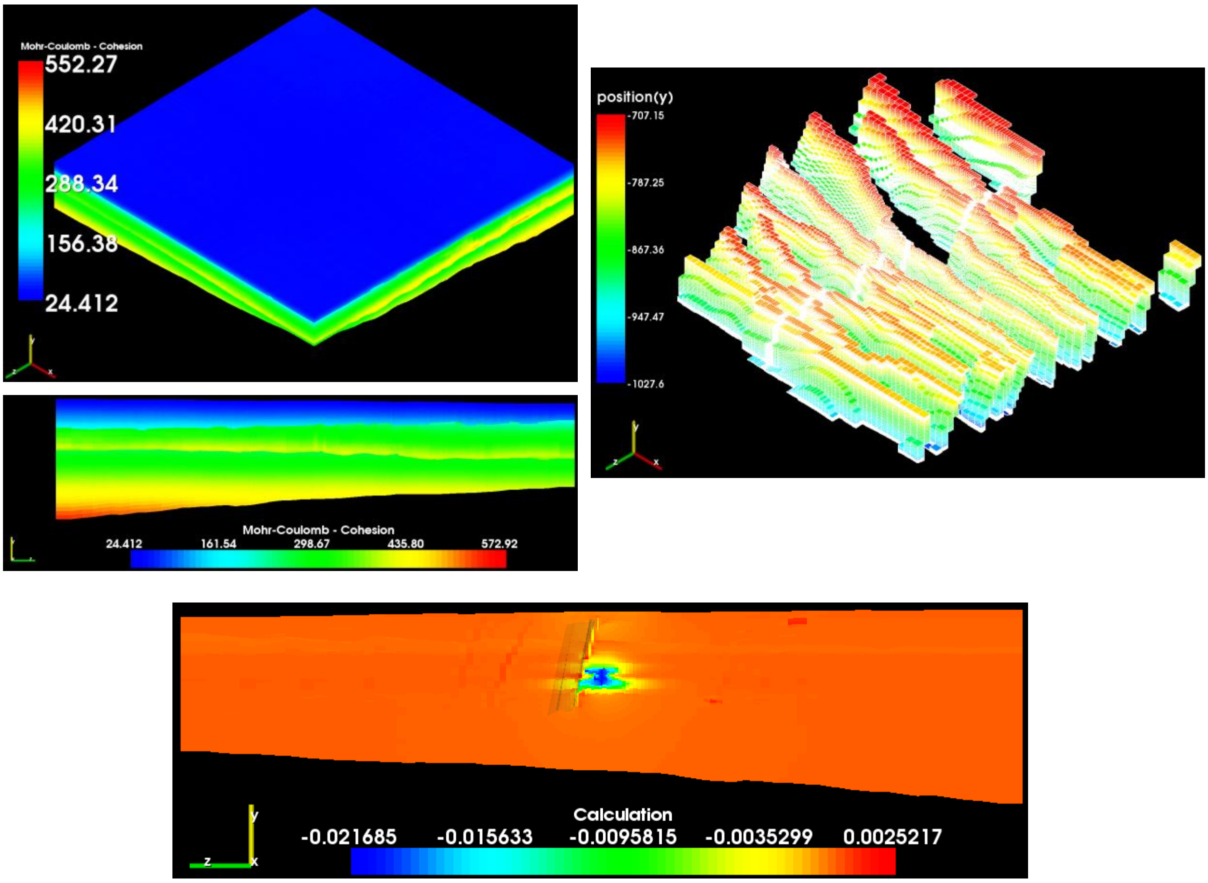


Fig. 5 An example of 3D geomechanical simulation result. Distribution of cohesion c (top-left), delineated faults (top-right) and of the effect of MH dissociation on fault (distribution of the volumetric strain) in a test site candidate (not Daini Atsumi). MH dissociation region was calculated by using a MH21-HYDRES simulator.

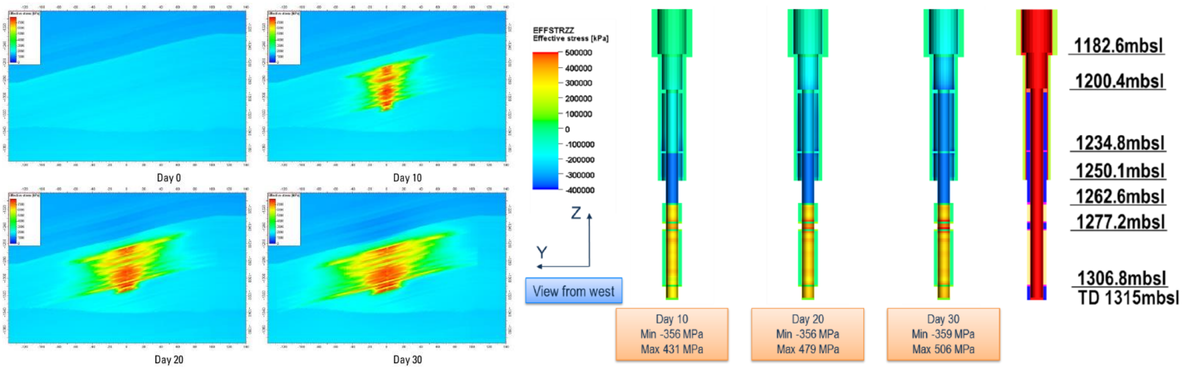


Fig. 6 Estimated effective stress distribution during the production test in the Daini Atsumi area (left) and AT1-P3 well (right).

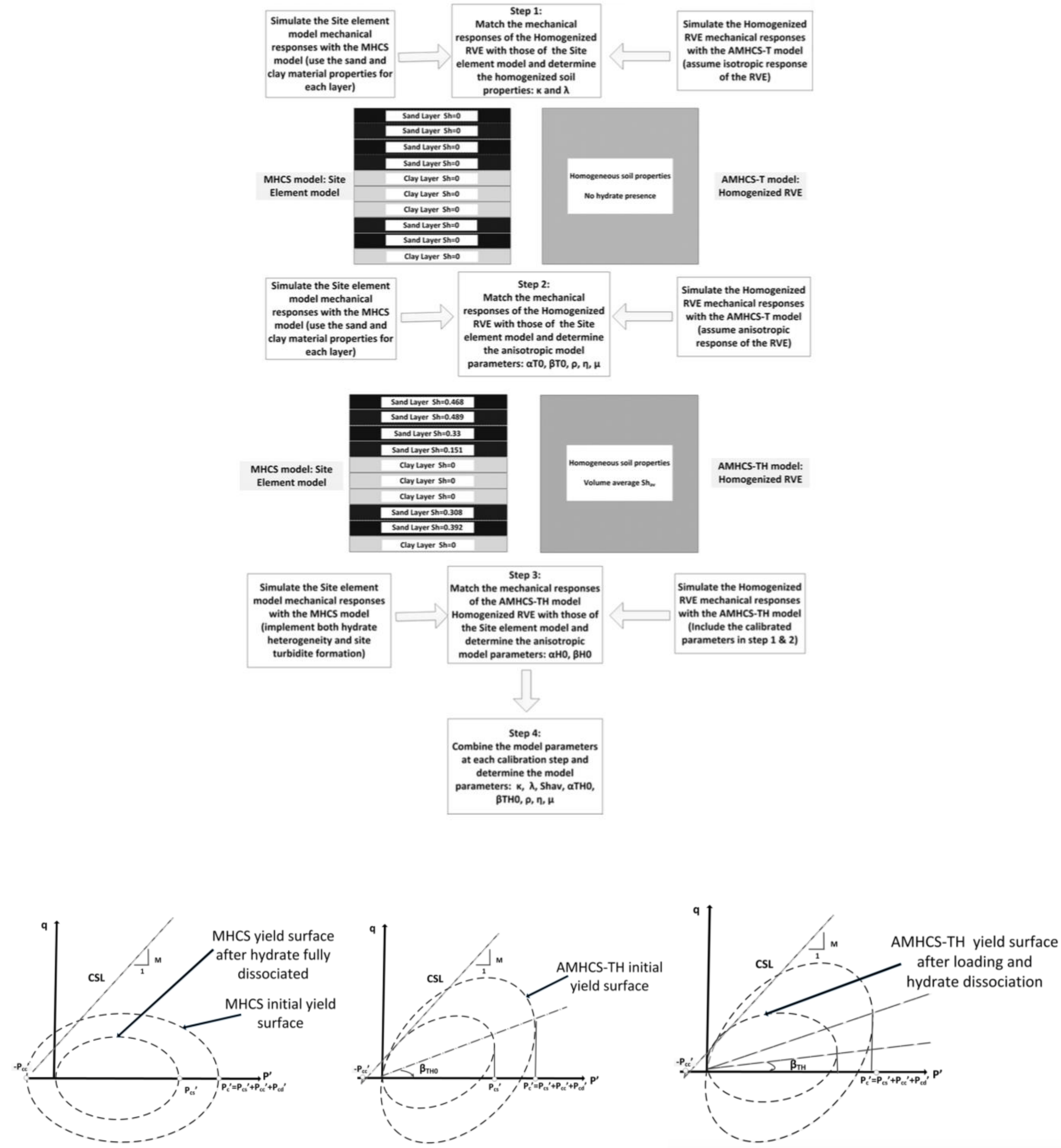


Fig. 7 Schematic flow of the process of homogenization (top) and yield surfaces of the homogeneous (bottom left), MH-bearing (bottom center), and MH dissociated (bottom right) medium.

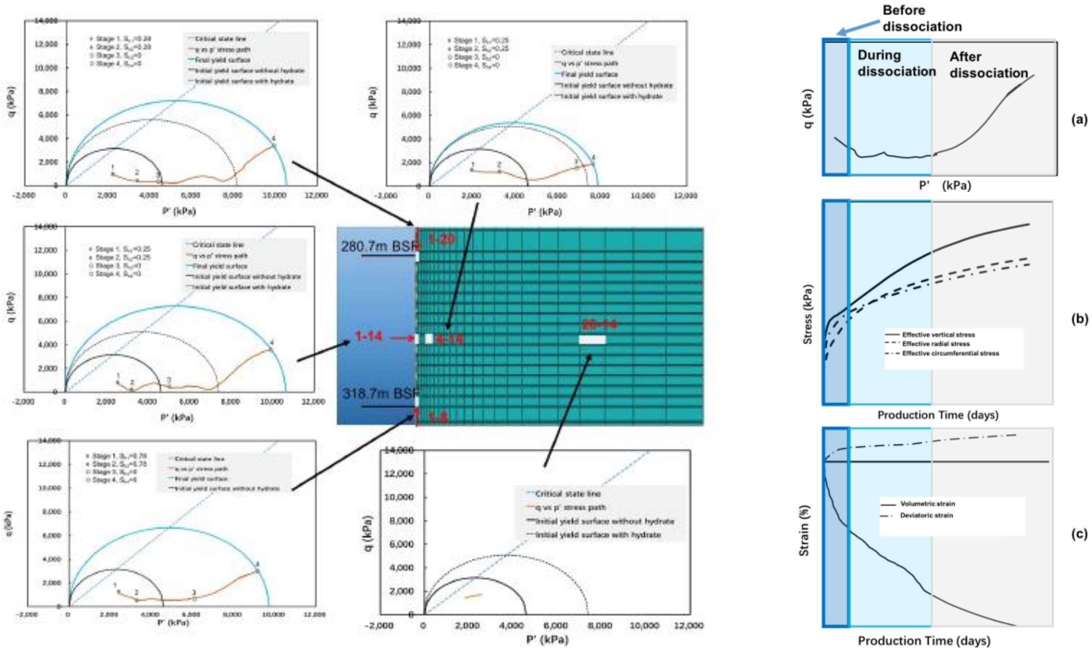

Fig. 8 Calculated stress state in the MHCZ and overburden/underburden zones (left) and stress and strain changes at some locations (Zhou et al., 2018b).

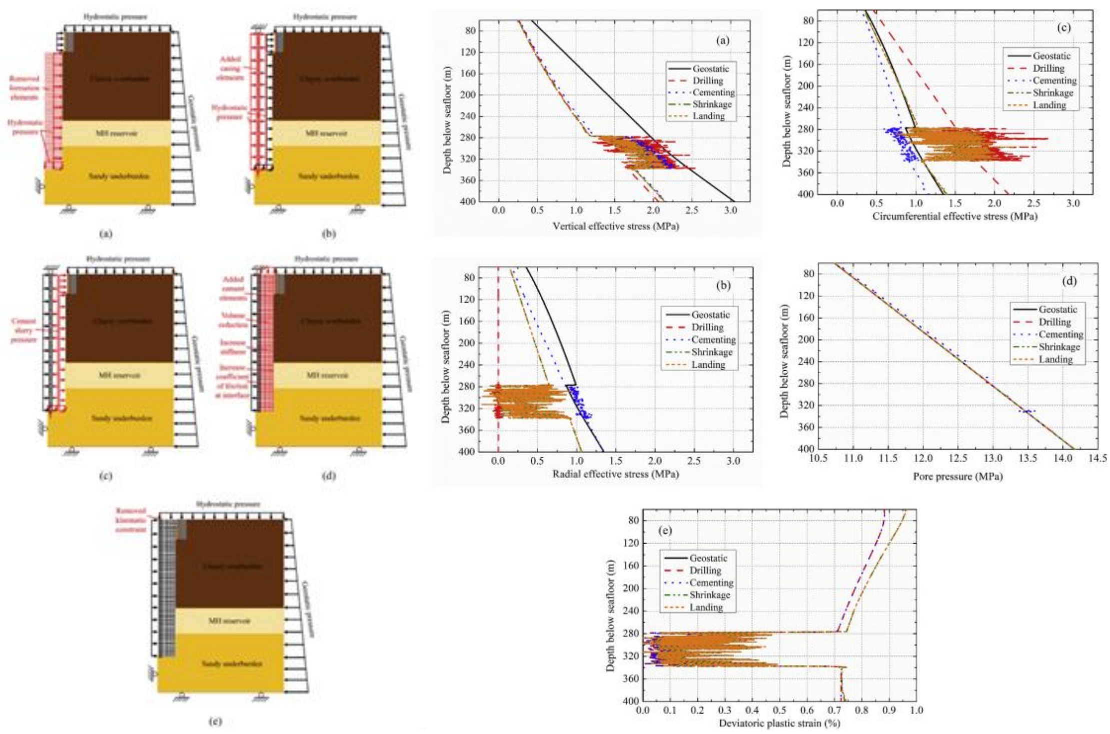

Fig. 9 Left: Model of the drilling stages (a: drilling, b: run casing, c: cementing, d: cement hydration, e: applying casing weight). Right: a: effective vertical stress, b: effective circumferential stress, d: pore pressure, e: deviatoric plastic strain of each stage.

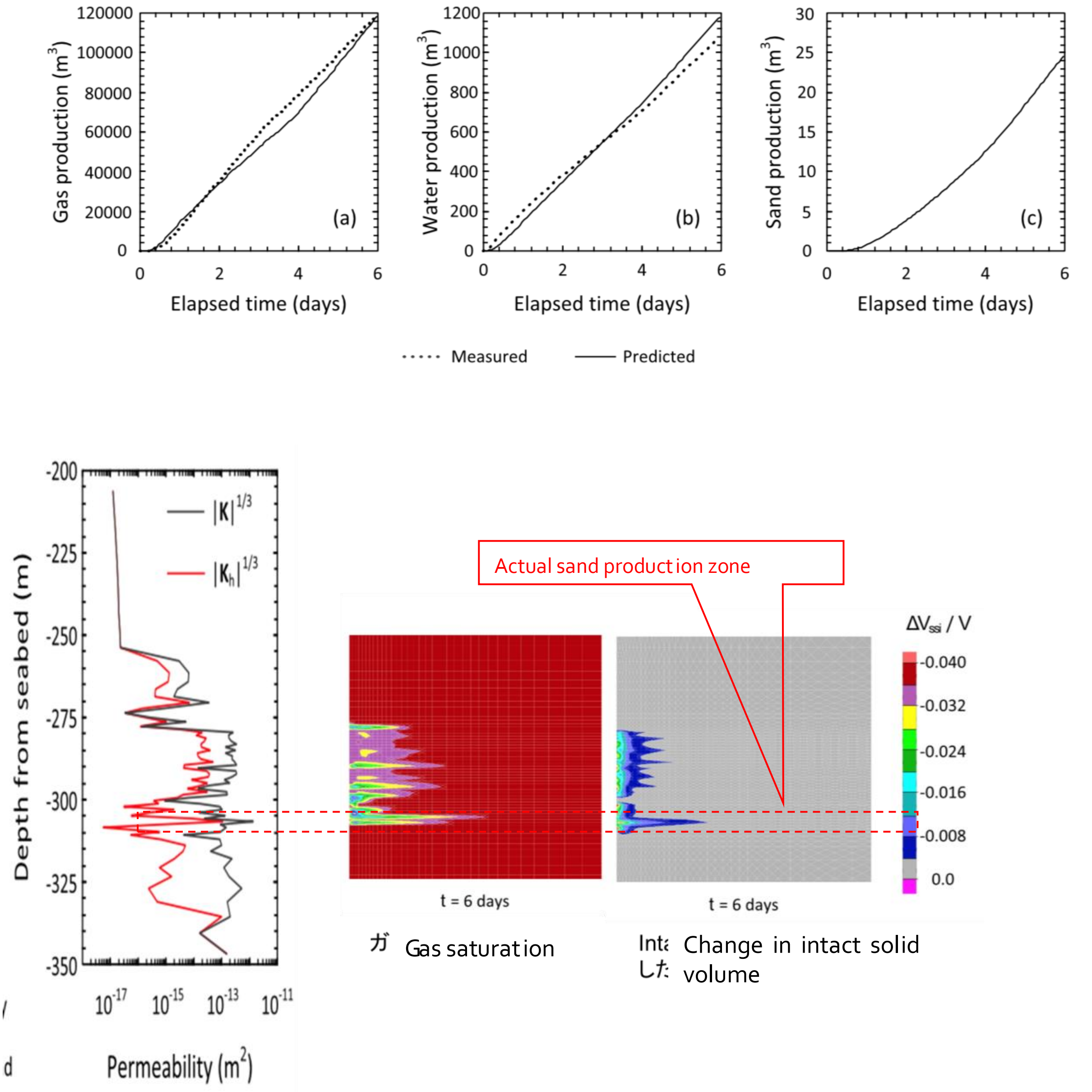


Fig. 10 History matching results of the gas, water and sand production volume of the first offshore production test (2013) using property data gathered from testing in the Eastern Nankai Trough. In the model, sand was produced continuously, however, during actual drilling, produced sand was trapped behind the screen and did not flow into the hole. Estimated sand production zone matches the observed sand produced interval (Yamamoto et al., 2017)

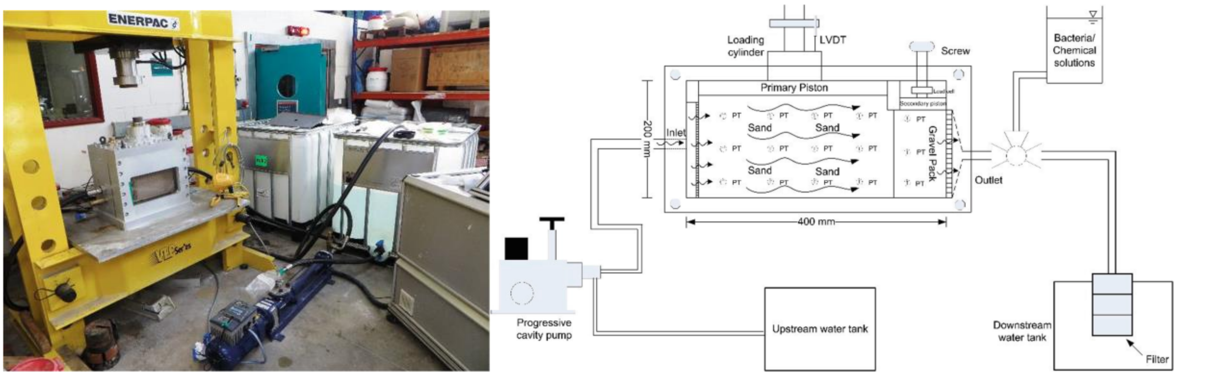


(1) MICP test device

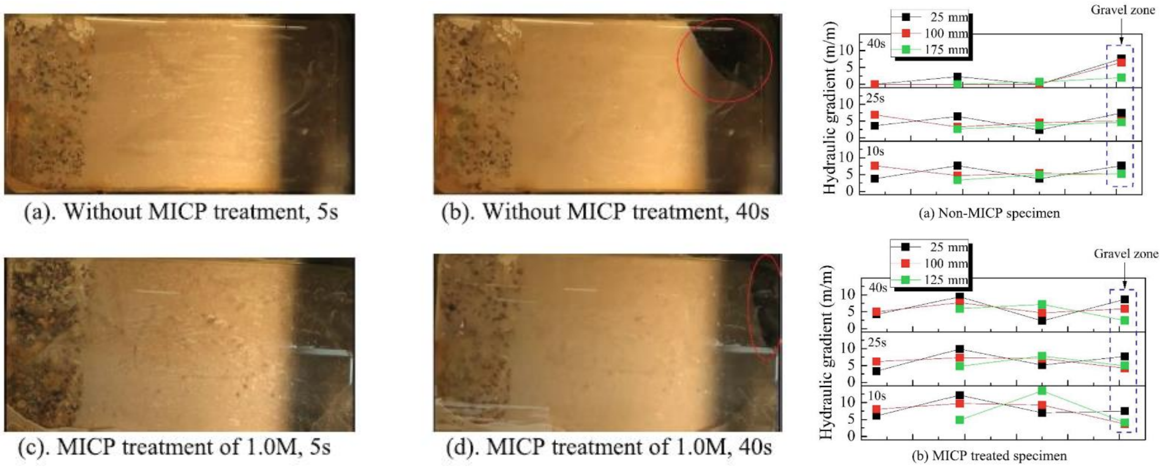


(2) Samples with different MICP treatment and hydraulic gradient distribution.

Fig. 11 MICP evaluation test device and test result that showed that the hydraulic condition change was relatively small in MICP treated specimens (Jiang et al., 2018).

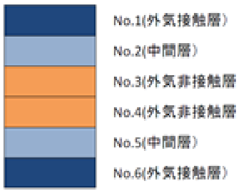


| 試験ケース名 | 尿素濃度 | 酵母エキス濃度 | 備考 |
|---|---|---|---|
| 1 | 0.15mol/L | 6.6g/L | 外気接触層 |
| 2 | | | 中間層 |
| 3 | | | 外気非接触層 |
| 4 | | | 外気非接触層 |
| 5 | | | 中間層 |
| 6 | | | 外気接触層 |

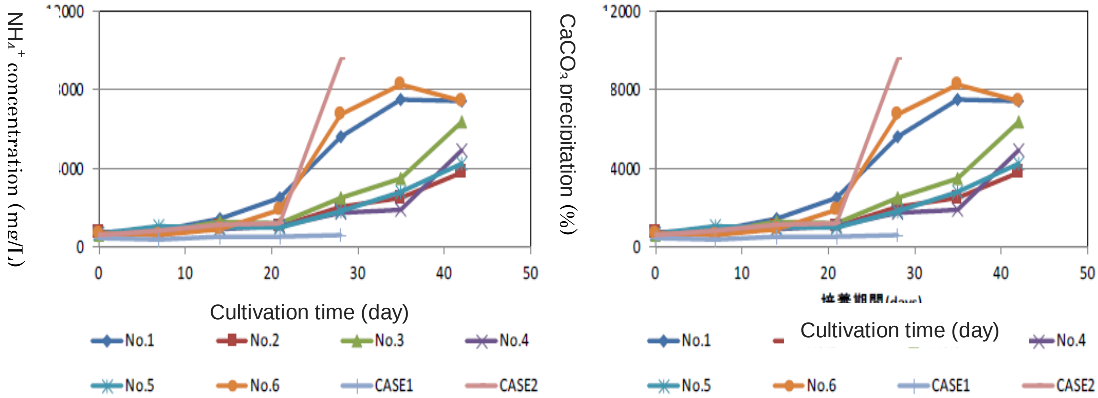


Fig. 12 Ammonium ion concentration (indication of urease active species) and calcite precipitation during cultivation done for pressure core samples (2018). The results indicate the existence of useful species and the effectiveness of MICP activities.

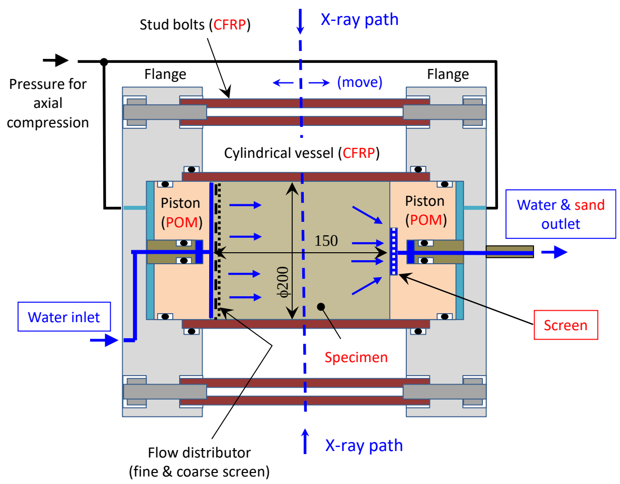


Fig. 13 Sand production test device used in X-ray CT

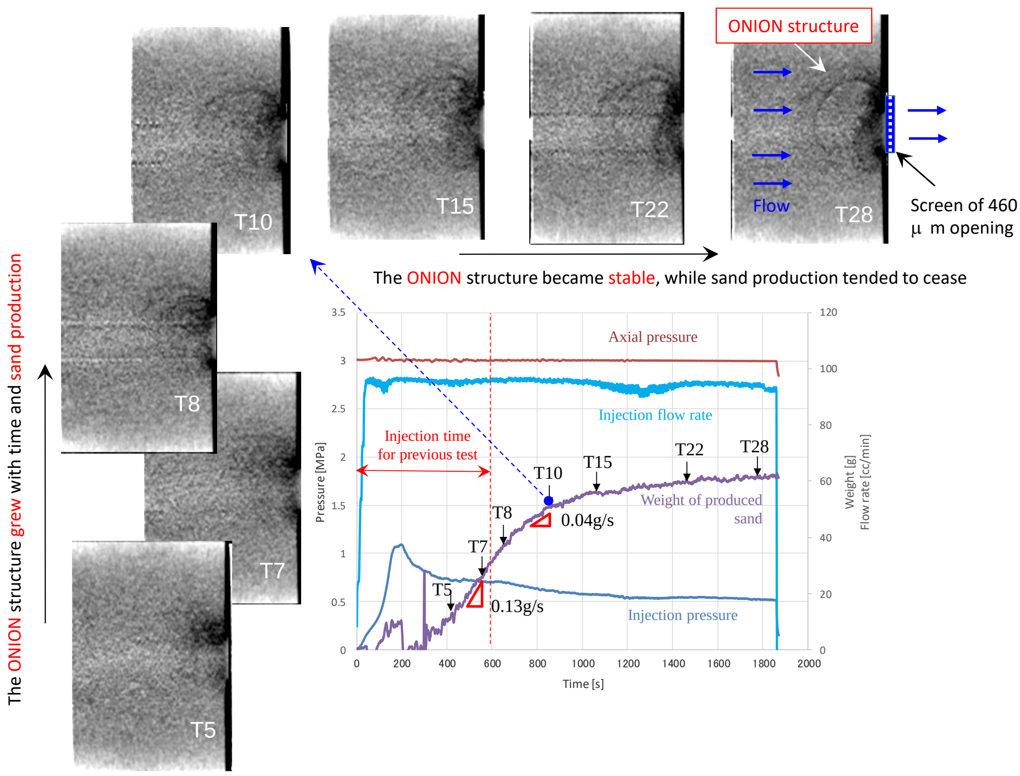


Fig. 14 A typical sand production test result (injection rate, pressure and sand weight and CT images of each step

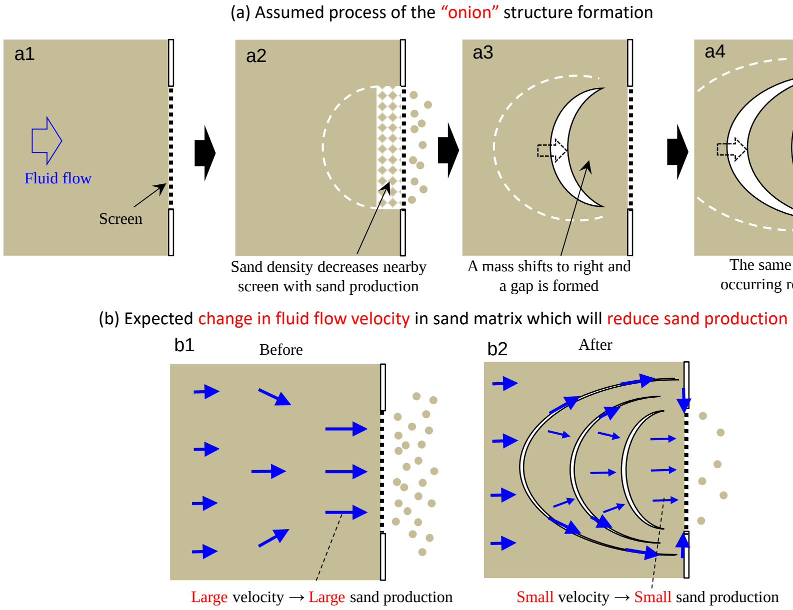


Fig. 15 Interpreted mechanism of sand stabilization

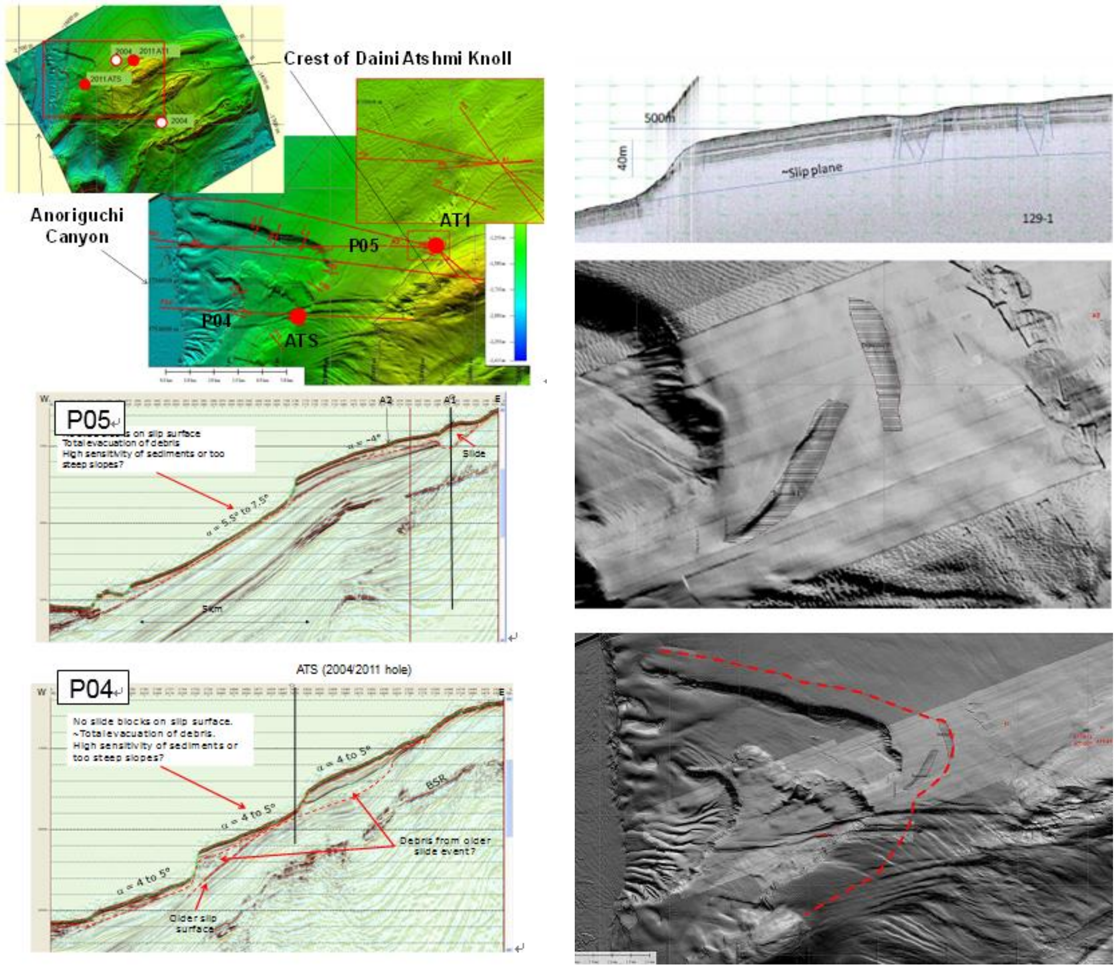


Fig. 16 Seismic cross section and bathymetry image of land slide scar area in the west of the offshore production test.

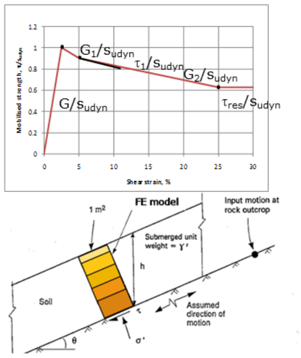


1D mechanical model in the slope for dynamic loading

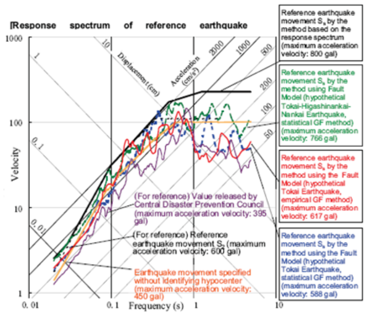


Assumed seismic ground motion Ss response spectrum (horizontal motion) for seismic safety assessment of Hamaoka Nuclear Power Station Reactor No. 4 (Chubu electric power, http://www.chuden.co.jp/english/corporate/press2006/0125_2_1.html)

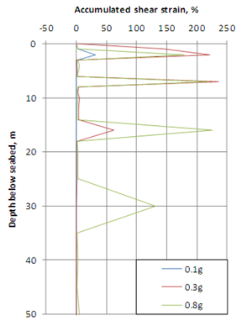


Accumulated plastic strain

Fig. 17 Evaluation of the effect of the anticipated earthquake on the stability of shallow formation.

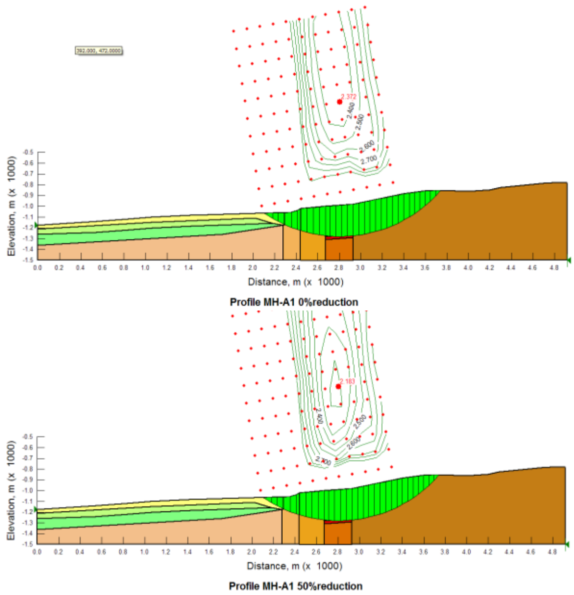


Change of Factor of safety by gas hydrate dissociation (50% reduction of shear strength). (FoS: 2.372→2.183)

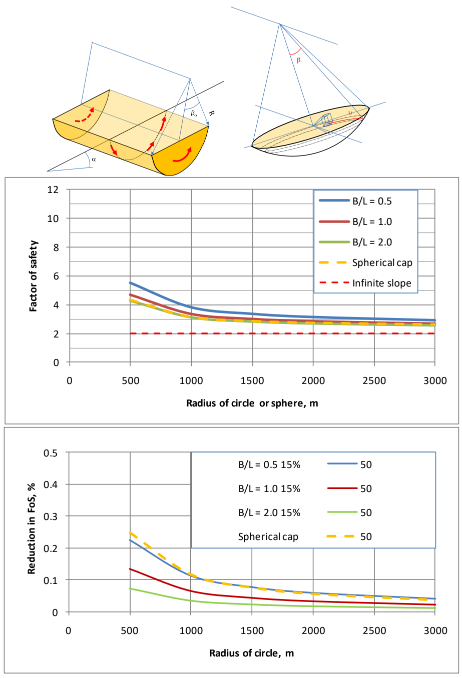


Relationship between slide types (spherical and cylindrical), scales of the slide and FoS reduction.

Fig. 18　Effect of MH dissociation (width=280m) on the factor of safety (FoS). Reduction of FoS is small under the small scale dissociation scenario.

References

Nagano, Y., Lin, W., Yamamoto, K. (2015): In-situ stress analysis using the anelastic strain recovery (ASR) method at the first offshore gas production test site in the eastern Nankai Trough, Japan, Marine and Petroleum Geology, 66, Part 2, 418-424.

Yamamoto, K., Murray, D., Khong C.-K., Yasuda, M. & Nakamizu, M. 2006. Geomechanics data acquisition techniques used in the METI Tokai-oki to Kumano-nada drilling campaign, the *12 th Formation Evaluation Symposium of Japan.*

Tarantola, A., Tarantola, A., 1987, Inverse problem theory; methods for data fitting and model parameter estimation, Elsevier (1987)

Qiu, K., Yamamoto, K., Birchwood, R.A., Chen Y.-R., Wu, C., Tan, C.-P. & Singh, V. 2012. Evaluation of Fault Re-activation Potential during Offshore Methane Hydrate Production in Nankai Trough, Japan, *OTC*-22890-MS, Offshore Technology Conference, Houston, Texas, USA, 30 April-3 May, 2012.

Uchida, S., et al. (2012) J. Geophys. Res.: Solid Earth (1978–2012), 117(B3).

Wheeler, S. J., et al., (2003). Canadian Geotechnical Journal, 40(2):403–418.

Wongsaroj, J. (2006). PhD thesis, University of Cambridge.

Zhou M, Soga K., Yamamoto K. (2018a), Upscaled Anisotropic Methane Hydrate Critical State Model for Turbidite Hydrate-Bearing Sediments at East Nankai Trough, JGR Solid Earth, 30 July 2018, https://doi.org/10.1029/2018JB015653

Zhou, M., Soga, K., Yamamoto,K. Huang, H. (2018b), Geomechanical responses during depressurization of hydrate-bearing sediment formation over a long methane gas production period. Geomech. Energy Env. In press, https://doi.org/10.1016/j.gete.2018.12.002.

Sasaki, T., Soga, K., Abuhaikal, M. 2018a: Simulation of wellbore construction in offshore unconsolidated methane hydrate-bearing formation, J. Petrol.Sci. Eng., 169, 205–219.

Sasaki, T., Soga, K., Elshafie, M.Z.E.B 2018b: Water absorption and shrinkage behaviour of early-age cement in wellbore annulus, J. Natural Gas Sci. Eng., 60 (2018) 312–326.

Uchida, S, Klar, A, Yamamoto, K (2016a): Sand production model in gas hydrate-bearing sediments, International Journal of Rock Mechanics and Mining Sciences 86:303-316: DOI: 10.1016/j.ijrmms.2016.04.009

Uchida, S., Klar, A. and Yamamoto, K. (2016b): Sand production modeling of the 2013 Nankai offshore gas production test. In: F. Wuttke, S. Bauer & M. Sanchez (eds.) 1st International Conference on Energy Geotechnics, 29-31 August, Kiel, Germany. 451-458.

Jiang, N..-J., Soga, K., Yoshioka, H., Yamamoto, K. (2016): Ureolytic activities of a urease-producing bacterium and purified urease enzyme in the anoxic condition: Implication for subseafloor sand production control by microbially induced carbonate precipitation (MICP) , Ecological Engineering, 90, 96-104.

Jiang, N..-J., Soga, H., Yamamoto, K. (2018): A High-Pressure Plane-Strain Testing System to Evaluate Microbially Induced Calcite Precipitation as a Sand Production Control Method, GeoShanghai 2018 International Conference: Geoenvironment and Geohazard, May 27-30, Shanghai, China.

Ito, T. and Nagano, Y., Laboratory Study of Sand Production in Unconsolidated Sands by Using X-ray CT for Methane Hydrate Development, SPE Workshop“Sand Management Workshop”, Kuala Lumpur, (2016.4.25-26).

Kvalstad, T.J. (2010): Seafloor stability, International Symposium on Methane Hydrate Resources, MH21 Research Consortium, Tokyo, Japan.